OXFORD UNIVERSITY PRESS | Carcinogenesis

DNMT3A epigenetically regulates key microRNAs involved in epithelial-to-mesenchymal transition in prostate cancer

Journal:	*Carcinogenesis*
Manuscript ID	CARCIN-2021-00015.R2
Manuscript Type:	Original Article
Date Submitted by the Author:	13-Aug-2021
Complete List of Authors:	Mancini, Monica; University of Insubria, Dept. of Biotechnology and Life Sciences Grasso, Margherita; University of Trento Centre for Integrative Biology, Department of Cellular, Computational and Integrative Biology Muccillo, Livio; University of Sannio of Benevento, Dipartimento di Scienze e Tecnologie (DST) Babbio, Federica; University of Insubria, Dept. of Biotechnology and Life Sciences Precazzini, Francesca; University of Trento Centre for Integrative Biology, Department of Cellular, Computational and Integrative Biology Castiglioni, Ilaria; University of Insubria, Dept. of Biotechnology and Life Sciences Zanetti, Valentina; University of Insubria, Dept. of Biotechnology and Life Sciences Rizzo, Francesca; University of Salerno - Baronissi Campus, Department of Medicine, Surgery and Dentistry ; University of Salerno - Baronissi Campus, Genome Research Center for Health Pistore, Christian; University of Insubria, Dept. of Biotechnology and Life Sciences de Marino, Maria Giovanna; University of Insubria, Dept. of Biotechnology and Life Sciences Zocchi, Michele; University of Insubria, Dept. of Biotechnology and Life Sciences Del Vescovo, Valerio; University of Trento Centre for Integrative Biology, Department of Cellular, Computational and Integrative Biology Licursi, Valerio; Sapienza University of Rome, Dept. of Biology and Biotechnology "Charles Darwin" Giurato, Giorgio; University of Salerno - Baronissi Campus, Department of Medicine, Surgery and Dentistry ; University of Salerno - Baronissi Campus, Genome Research Center for Health Weisz, Alessandro; University of Salerno - Baronissi Campus, Department of Medicine, Surgery and Dentistry ; University of Salerno - Baronissi Campus, Genome Research Center for Health Chiarugi, Paola; University of Florence, Department of Biomedical, Experimental and Clinical Sciences 'Mario Serio' Sabatino, Lina; University of Sannio of Benevento, Dipartimento di Scienze e Tecnologie (DST) Denti, Michela; University of Trento Centre for Integrative Biology, Department of Cellular, Computational and Integrative Biology

	Bonapace, Ian; University of Insubria, Dept. of Biotechnology and Life Sciences
Keywords:	DNMT3A, Epithelial-to-mesenchymal transition, microRNAs, Prostate cancer

DNMT3A epigenetically regulates key microRNAs involved in epithelial-to-mesenchymal transition in prostate cancer

Monica Mancini[1, †], Margherita Grasso[2a, †], Livio Muccillo[3, †], Federica Babbio[1], Francesca Precazzini[2], Ilaria Castiglioni[1b], Valentina Zanetti[1c], Francesca Rizzo[4, 5], Christian Pistore[1], Maria Giovanna De Marino[1], Michele Zocchi[1], Valerio Del Vescovo[2d], Valerio Licursi[6], Giorgio Giurato[4, 5], Alessandro Weisz[4, 5], Paola Chiarugi[7], Lina Sabatino[3], Michela Alessandra Denti[2], Ian Marc Bonapace[1, *]

[1] Department of Biotechnology and Life Sciences, University of Insubria, 21052 Busto Arsizio (VA), Italy

[2] Department of Cellular, Computational and Integrative Biology (CIBIO), University of Trento, Povo (TN), Italy

[3] Department of Sciences and Technologies, University of Sannio, 82100 Benevento, Italy

[4] Laboratory of Molecular Medicine and Genomics, Department of Medicine, Surgery and Dentistry 'Scuola Medica Salernitana', University of Salerno, 84081 Baronissi, Italy

[5] Genome Research Center for Health, c/o University of Salerno Campus of Medicine, 84081 Baronissi (SA), Italy

[6] Department of Biology and Biotechnology "Charles Darwin", "Sapienza" University of Rome, Rome, Italy

[7] Department of Biomedical, Experimental and Clinical Sciences '*Mario Serio*', University of Florence, Florence, Italy

[a] Present address: L.N.Age Srl, 00040 Pomezia (RM), Italy

[b] Present address: laboratory of Gene Expression and Muscular Dystrophy, San Raffaele Scientific Institute, Milan, Italy

[c] Present address: ICON Plc, 20159 Milano, Italy

[d] present address: Exom Group Srl, 20124 Milano, Italy

* To whom correspondence should be addressed. Tel: +39 0331339452; Email: ian.bonapace@uninsubria.it

Correspondence may also be addressed to Michela Alessandra Denti, Tel: +39 0461283820; Email: michela.denti@unitn.it

[†] These authors contributed equally to this work.

Abstract

Epithelial-to-Mesenchymal Transition (EMT) is involved in prostate cancer metastatic progression, and its plasticity suggests epigenetic implications. Deregulation of DNMTs and several miRNAs plays a relevant role in EMT, but their interplay has not been clarified yet.

In this study we provide evidence that DNMT3A interaction with several miRNAs has a central role in an *ex-vivo* EMT prostate cancer model obtained via exposure of PC3 cells to conditioned media from cancer-associated fibroblasts (CM-CAFs). The analysis of the alterations of the miRNA profile shows that miR-200 family (miR-200a/200b/429, miR-200c/141), miR-205, and miR-203, known to modulate key EMT factors, are downregulated and hyper-methylated at their promoters. DNMT3A (mainly isoform a) is recruited onto these miRNA promoters, coupled with the increase of H3K27me3/H3K9me3 and/or the decrease of H3K4me3/H3K36me3.

Most interestingly, our results reveal the differential expression of two DNMT3A isoforms (a and b) during *ex-vivo* EMT and a regulatory feedback loop between miR-429 and DNMT3A that can promote and sustain the transition toward a more mesenchymal phenotype. We demonstrate the ability of miR-429 to target *DNMT3A* 3'UTR and modulate the expression of EMT factors, in particular ZEB1. Survey of the PRAD-TCGA data set shows that patients expressing an EMT-like signature are indeed characterized by down-regulation of the same miRNAs with a diffused hyper-methylation at miR-200c/141 and miR-200a/200b/429 promoters. Finally, we show that miR-1260a also targets DNMT3A, although it does not seem involved in EMT in prostate cancer.

Summary

In an *ex-vivo* prostate cancer model of EMT, DNMT3A determines promoter methylation of miRNAs regulating key EMT factors. Analysis of TCGA-PRAD patients with an EMT signature confirms these findings, supporting the role of DNMT3A in EMT and PCa progression.

Running Head

DNMT3A and miRNAs interplay during EMT in PCa

Introduction

Prostate cancer (PCa) is the most diagnosed cancer among men and the third/second leading cause of cancer-related deaths in Europe/United States, respectively (1,2). Current treatments for primary prostatic tumour involve radical prostatectomy, radiotherapy and androgen deprivation therapy (ADT) (3). However, after an initial response, patients become refractory to ADT, developing castration-resistant PCa (CRPC) which frequently leads to metastasis and eventually to death (3). Epithelial-to-mesenchymal transition (EMT) has been shown to be a relevant process to CRPC (4). For the transition to a complete mesenchymal state, EMT requires intermediate steps, which define metastable or stable phenotypes that depend on the persistence of EMT promoting signals (5). This plasticity suggests that the epigenetic landscape is implicated in the transition dynamics (6).

Altered DNA methylation patterns are early and consistent molecular changes of human tumours (7-10), contributing to several aspects of PCa progression (11,12). DNA methyltransferases (DNMTs) (13) and UHRF1, a reader/writer of histone marks required for proper localization of DNMT1 (14), have a central role in epigenetic gene regulation: DNMT1/UHRF1 are involved in the methylation-maintenance of newly synthesised DNA strands following replication; DNMT3A and 3B are responsible for *de novo* DNA methylation at selected loci (15). DNMTs have been found to be deregulated in several tumours (10,16) and their expression and activity are elevated in prostate tumour models, as well as in androgen-resistant prostate cancer cell lines (17,18). We have recently shown that, in an *ex-vivo* model of EMT, conditioned media from patient-derived cancer-associated fibroblasts (CM-CAF) downregulates DNMT1/3B and UHRF1 in androgen-resistant PC3 cells, but not in androgen-responsive LNCaP cells (6). In our model, DNMT3A is pivotal: this methyltransferase is not repressed during the transition and is required for EMT by methylating the promoters of key epithelial factors, such as CDH1. These results underline the plasticity of the epigenetic regulation in sustaining and promoting cancer processes.

MicroRNAs (miRNAs) are endogenous non-coding short single-stranded RNAs that negatively regulate gene expression at the post-transcriptional level, either by degrading or inhibiting translation of the target mRNA (19). Deregulation of miRNA expression profile is associated with numerous human tumours, including prostate cancer (20,21); they act as onco-miRNA or tumour suppressors miRNA depending on their target genes (22). Among the latter, the miR-29 family regulates DNMT3A expression in several tissues (23) and during EMT (6). Genomic rearrangements, hyper-methylation of CpG island-containing promoters or transcriptional deregulation mechanisms can alter the expression of miRNAs, linking them to the initiation/promotion of the neoplastic process (24-26). Several miRNAs are known to

target EMT factors and reported to be markedly down-regulated during PCa progression, contributing to the mesenchymal phenotype. Re-expression of miR-203, miR-205 and miR-29b is known to restore the epithelial phenotype in PCa cell lines by negatively regulating EMT factors; the transcriptional repressor ZEB1 controls miR-200 family expression in breast cancer (24,27-30) and is a target of the same miRNA family (31,32).

To better clarify the role of DNMT3A in EMT, we investigated its interplay with different miRNAs in castration-resistant PCa, and their link to the EMT program associated with permanent changes in DNA methylation and expression of miRNAs (6).

Materials and methods

Cell cultures

Human PCa cell lines, PC3 (RRID:CVCL_0035) and LNCaP (RRID:CVCL_1379), were obtained from American type culture collection (ATCC, Manassas, VA, USA) in 2016 and cultured following the instructions of the company. All were authenticated using short tandem repeat profiling by ATCC, propagated, expanded, and frozen immediately. Revived cells were utilized within 10 to 12 passages (not exceeding a period of 3 months) and regularly tested for mycoplasma contamination (N-GARDE Mycoplasma PCR Reagent set, EuroClone, Milan, IT). Both cell lines were cultured in RPMI 1640 (EuroClone) supplemented with 10% heat-inactivated foetal bovine serum (EuroClone), 2 mM glutammine and 100 U/ml penicillin/ streptomycin (EuroClone).

Ex-vivo EMT induction

EMT induction was performed exposing PC3 cells for 72 h to conditioned media of cancer-associated fibroblasts (CM-CAFs) or benign hyperplastic fibroblasts (CM-HPFs, control), following the published protocol (6).

Western blot analysis

Whole cell extracts were separated on 8-14% SDS-PAGE gels (BioRad, and transferred to nitrocellulose membranes, then incubated with primary antibodies: DNMT3A (Active Motif, Carlsbad, CA, USA), DNMT3A2 (Merck Millipore, Burlington, MA, USA), E-CAD and N-CAD (Novus Biological, Littleton, CO,

USA), VIM (GeneTex, Irvine, CA), ZEB1 (Cell Signaling Technology, Danvers, MA, USA). Chemiluminescence reactions on secondary anti-mouse and anti-rabbit antibodies (Jackson ImmunoResearch Laboratories, West Grove, PA, USA) was detected using ECL western blotting reagents (GE Healthcare Amersham, Chicago, IL, USA). Equal loading was checked using GAPDH (Merk Millipore).

RNA sequencing and genome-wide DNA methylation analysis

Analysis of RNA sequencing and genome-wide DNA methylation were performed on previously published experiments (6), respectively using HiSeq2500 platform (Illumina, San Diego, CA, USA) with a coverage of >70 million sequence reads per sample and HumanMethylation 450 K BeadChip (Illumina), which covers 21 231 (99%) RefSeq genes. For small RNA sequencing, 1 ug of total RNA was used for indexed sequencing library preparation with a TruSeq small RNA Sample Prep Kit (Illumina) and sequenced on HiSeq1500 (Illumina) for 50 cycles.

Chromatin Immunoprecipitation analysis

Chromatin immunoprecipitation (ChIP) was performed as previously published (6). Briefly, cells were treated with 1% formaldehyde, then 0.125 M glycine was added. The cells were collected in PBS, re-suspended in lysis buffer and sonicated (BRANSON S250 digital sonicator, Branson, Danbury, CT, USA). Pre-cleared chromatin was quantified using Qubit (dsDNA BR Assay Kit, Life Technologies); 2 ug chromatin was incubated overnight at 4°C with anti-IgG (Santa Cruz Biotechnology, Dallas, TX, USA), anti-DNMT1, -DNMT3A, -DNMT3B, and anti-H3K9me3, -H3K27me3, -H3K4me3 and -H3K36me3 (all Active Motif). Ten percent of the total lysate was used for input control. DNA was extracted with the Chromatin IP DNA extraction kit (Active Motif) following the manufacturer protocol. Immunoprecipitation products were amplified using iTAq Polymerase (Bio-Rad, Hercules, CA, USA) and specific primers (Supplementary Table 1B).

PRAD TCGA data set analysis

A primary prostate adenocarcinoma (PRAD) dataset of 494 patients retrieved from of The Cancer Genome Atlas (TCGA) consortium was enquired (https://gdc-portal.nci.nih.gov). IlluminaHiSeq mRNA-Seq expression was used to classify patients presenting EMT or MET features. Each patient was assigned a reward or penalty score for each EMT/MET gene considered. EMT-like phenotype was

defined as high levels (>Q3 or Q4, Q=quartile) of EMT genes (ZEB1, VIM, SMO, SHH, LGR5 and HEY) and low levels (<Q1 or Q2) of MET genes (CDH1, GRHL2, OVOL1/2 and ESPR1); MET-like phenotype displayed the opposite signature. Reward scores were assigned for each gene when the above-mentioned conditions were met, and penalty scores were assigned when they were disregarded. Only patients with resulting positive scores for EMT or MET were chosen, assigned to EMT-like or MET-like subgroup (47 and 40 cases, respectively) and subsequently analysed by comparing cytosines DNA methylation (Illumina, HumanMethylation 450K array) and the smallRNA-Seq expression (IlluminaHiSeq) with differentially expressed miRNAs from PC3 cell lines. The heatmaps illustrated in Figure 1B and Figure 3 were obtained using the publicly available software Morpheus (https://software.broadinstitute.org/morpheus/) and the 'One minus Pearson correlation' as miRNAs hierarchical clustering algorithm.

microRNA target prediction

Bioinformatic tools were used to identify miRNAs predicted to target *DNMT3A*-3'UTR: http://mirdb.org (33); http://www.targetscan.org (34); http://mirna.imbb.forth.gr (35) and http://comirnet.di.uniba.it:8080/ (36). Bioinformatic analyses of transcript accessibility and binding strength calculation were performed with PITA (https://genie.weizmann.ac.il/pubs/mir07/mir07_prediction.html) (37) to predict the presence of target sites for miRNAs on *DNMT3A*-3'UTR. The hybridization minimum free energy (mfe) for miRNAs' binding was calculated with RNAhybrid (https://bibiserv.cebitec.uni-bielefeld.de/rnahybrid/) (38).

RT-qPCR

Total RNA was extracted from cells using Trizol (Invitrogen, Waltham, MA, USA) and treated with Turbo DNA-free™ Kit (Applied Biosystem, Waltham, MA, USA). For miRNA analysis, RNA was reverse-transcribed using TaqMan®v MicroRNA Reverse Transcription Kit (Applied Biosystem) and miRNAs were measured following the TaqMan® MicroRNA Assays (Applied Biosystem) protocol: has-miR-200b (ID: 002251), has-miR429 (ID: 001024), hsa-miR-1260a (ID: 002896), hsa-miR-29a (ID: 002112), hsa-miR-29b (ID: 000413). U48 (RNU48, ID: 001006) was used as control. Real-time PCR reactions were carried out on a CFX Connect (BioRad) using Fast Start TaqMan probe Master (Roche Life Science, Penzberg, DE). For quantitative mRNA analysis, 1 ug of total RNA was reverse-transcribed using SuperScript III RT (Invitrogen) with oligo-dT primer according to manufacturer's instructions. Real-time

PCR were performed with 1X iQ™SYBR Green Supermix (Bio-Rad) as previously described (6). Levels of miRNAs or mRNAs expression were determined by Gene Expression Analysis for iCycler iQ Real-Time PCR Detection System v1.10 (Bio-Rad) according to the $2^{-\Delta\Delta Ct}$ method. Primers (Supplementary Table 1A; previous publication(6)) were designed with Primer3 (http://primer3.ut.ee/) and tested against public databases (NBLAST).

Dual-luciferase reporter assay

To generate the pGL4.13[luc2/SV40]-*DNMT3A*3'UTR vector (*DNMT3A*-3'UTR), the intact *DNMT3A*-3'UTR sequence (NM_175629, 1248nt) was amplified and cloned into Firefly luciferase expressing pGL4.13[luc2/SV40] reporter vector (Promega Corporation, Madison, WI, USA) using *FseI* restriction site. To generate the pGL4.13[luc2/SV40]-*DNMT3A⊿1260a*-3'UTR (Δ1260a_1, Δ1260a_2 and Δ1260a_1_2), the wild type *DNMT3A*-3'UTR plasmid was used as template. Mutated constructs were created using Quick-Change II XL Site-Directed Mutagenesis Kit (Stratagene, CA, USA), according to the manufacturer's protocol, with two complementary primers carrying the desired mutation (Supplementary Table 1A). The correct mutagenesis was verified by automated Sanger DNA sequencing (BMR Genomics, Padova, IT). RegRNA (http://regrna.mbc.nctu.edu.tw/) and UTRscan (http://itbtools.ba.itb.cnr.it/utrscan) were used to exclude creation of novel binding sites or regulatory elements. The miRNA constitutive-expression cassettes for miR-429, miR-1260a, miR-608 (negative control) and miR-29a (positive control) were generated by amplification of human genomic DNA (#G1471 Promega) with PCR (primers in Supplementary Table 1A). The genomic fragments containing the pre-miRNA were cloned in the *BglII* and *XhoI* sites of the psiUx plasmid (39). The same psiUx plasmid (42) was transfected in parallel as an additional negative control ("empty plasmid"). PC-3 cells were seeded and transfected at 60-70% confluence using FuGENE® HD Transfection Reagent (Promega) with 50 ng of the pGL4.13 constructs containing *DNMT3A*-3'UTR wild type or mutants and 450 ng of miRNA-overexpressing plasmids. To normalize Firefly luciferase activity, a vector containing the cDNA encoding Renilla luciferase (Rluc) was cotransfected (50 ng). 24 hours after transfection, cells were washed with PBS and lysed with Passive Lysis Buffer (Promega); Renilla and Firefly luciferase activity were measured using the Dual-Luciferase Assay System (Promega) in the Infinite® M200 (Tecan) plate reader.

Transfection of miRNA mimics and inhibitor LNAs

PC3 cells were seeded and transfected after 24h with mimic oligos (30 pmol miScript miRNA Mimic, QIAGEN, Hilden, DE, cat. n. 339173: miR-29a n. MSY0000086, miR-429 n. YM00472516, miR-1260a n. MSY0005911, AllStars n. 10027280) using Lipofectamine RNAiMax (Invitrogen), according to the manufacturer's recommendations. LNCaP cells were seeded and transfected after 24h with LNA (Locked Nucleic Acids) inhibitors (30 pMol miRCURY LNA™ miRNA Inhibitor, QIAGEN, cat n. 339121: Scramble ID: YI00199006, LNA-429 ID: YI04101290, LNA-1260a ID: YI04103217) using Lipofectamine RNAiMax (Invitrogen) transfection reagent, according to the manufacturers' protocol. Cells were harvested at different times depending on the specific assay.

Cell proliferation and wound-healing assays

PC3 and LNCaP cells were transfected as reported above. Starting 3 days after transfection cells were harvested and counted every 24 hours to evaluate cell growth. Simultaneously, a wound was created and observed using an Olympus BX81-inverted microscope. Images were taken by a UPlanFl 10X objective at regular intervals over the 24-48h course and acquired by a colour CCD camera (MicroPublisher 5.0) and the Qcapture pro software (Qimaging, Surrey, BC, Canada). Precise positioning of the samples for image acquisition was achieved by a motorized stage system (Optiscan II, Prior scientific instruments, Cambridge, UK). Images were analysed using imageJ (https://imagej.nih.gov/ij/) or Photoshop (Adobe); cell migration distance was determined by measuring the width of the wound and the cell-free area, normalised at each time point to the control.

microRNA microarrays

100 nanograms of total RNA samples was processed and hybridized to Human miRNA V2 Microarray 8 × 15K (G4470B, Agilent Technologies) using the miRNA Microarray System labelling kit V2 (Agilent 5190-0456), according to the manufacturer's instructions. Hybridized microarray slides were scanned with an Agilent DNA Microarray Scanner G2505C and data was analysed with the Agilent ScanControl version 8.1.3 software. The scanned TIFF images were background corrected using the Agilent Feature Extraction Software version 10.7.7.1. The raw data were normalized to the 75th percentile signal intensity as recommended by the vendor. After normalization all negative signal values were replaced by 0.01 and the values from multiple replicate spots for each miRNA were summarized as median signals which were used subsequently for statistical analyses. The pairwise Welch's T-test was used to identify significantly deregulated miRNAs. The significance thresholds in Welch's T- test were set to $p<0.05$,

|FC|.3 and a mean signal of all samples .50th percentile. Statistical and hierarchical clustering analyses (HCA) were done with the ArrayTrack Software (40).

Data analysis

Results are presented as mean ± s.d. of at least three independent biological and technical replicates. Statistical tests for each experiment are indicated in Figure Legends. P values ≤0.05 were considered statistically significant (*p<0.05, **p<0.01, ***p<0.001, ****p<0.0001).

Results

Comprehensive profile of miRNA alterations during CM-CAF induced EMT in prostate cancer cells.

Several miRNAs are known to be involved in EMT and markedly up- or down-regulated during PCa progression, through the regulatory activity of transcriptional factors such as ZEB1 or the hyper/hypo-methylation of their promoter regions (24,29). We recently reported that DNMT1, DNMT3B, and UHRF1 are deregulated in PC3 cells undergoing EMT mediated by exposure to conditioned media from cancer-associated fibroblasts (CM-CAFs), but not in PC3 CM-HPF (benign hyperplastic fibroblasts) (6). DNMT3A protein levels are the only slightly upregulated, and DNMT3A-dependent alterations in DNA methylation are pivotal for the transition.

Given these published results, we sought to obtain the comprehensive profile of epigenetic alterations following EMT induction; in first instance, we investigated the mechanisms transcriptionally regulating DNMT3A in our model, focusing on its promoter sequence. We previously demonstrated the selective methylation of DNMT3A variant 2 promoter (DNMT3A2, corresponding to isoform b) in CM-CAFs compared to CM-HPFs (6). In Figure 1A (left panel), mRNA analysis shows higher levels of DNMT3A2, compared to DNMT3A1, in non-treated (NT) PC3 cells, CM-HPF and CM-CAF. Despite the persistence of high levels of DNMT3A2 in all conditions, we observed that exposure to CM-CAF resulted in significant increase of DNMT3A1 (variant 1-3, isoform a) and decrease of DNMT3A2 (Figure 1A, central panel), which contribute to the slight (non-significant) increase of the DNMT3A (pan) total levels observed, as reported in our previous publication (6). At the protein level, we observed an even more marked shift between the two isoforms (Figure 1A, right panel, and Supplementary Figure 1A).

Focusing on the effects of *ex-vivo* EMT on the miRNome, we evaluated miRNA changes through RNA Sequencing and Methylation array. A total of 1276 miRNAs were detected in the two conditions. Compared to CM-HPF, CM-CAF induces in PC3 cells the deregulation of 302 miRNAs (differentially expressed – DE, p-value <0.05), as illustrated in Figures 1B and 1C. Among these, 284 showed fold change (FC) ⩾1.5 or ⩽-1.5 (Supplementary Table 2A and 2B). By analysing the DE miRNAs subsets, we recognized numerous miRNAs involved in the regulation of EMT pivotal players: in particular, the miR-200 family (miR-200a/200b/429, miR-200c/141), miR-205 and miR-203.

To investigate whether miRNAs deregulation was dependent on DNA methylation variations, we analysed the previously obtained Illumina HumanMethylation 450 K BeadChip data from PC3 CM-CAFs/CM-HPFs (6). DE and differentially methylated (DM, with Δβ-value ⩾0.2 or ⩽−0.2 and FDR≤0.05) miRNAs were classified as DM up-regulated and DM down-regulated (Figure 1D). We graphically divided the DM-5meC into four gates (G1, G2, G3 and G4) as previously reported (Figure 1D, see legend for definitions) (6). Around 90% of the DM cytosines were hypo-methylated (G1+G2 gated), while only 4.5% were G4-gated, corresponding to cytosines with a β-value <0.2 in CM-HPFs and >0.2 in CM-CAFs, and therefore *de novo*-methylated (G4 plots, Figure 1D).

These results demonstrate that in PC3 cells EMT induction, mediated by microenvironmental stimuli, is associated with a switch in DNMT3A isoforms and strong transcriptional and epigenetic alterations of the miRNome.

Recruitment of DNMT3A to the promoters of miR-200a/200b/429, -203 and -205a, and of miR-200c/141 during EMT.

In order to investigate the role of DNMT3A (especially isoform a, significantly increased in our model) in the alteration of the miRNA profile in our *ex-vivo* model, we focused our analysis on the hyper- and *de novo*-methylated cytosines (G3+G4 gated). We observed that the DM cytosines of miR-203 and miR-205 promoters, together with those of miR-200a/200b/429, are clustered in G4 gate in our experimental setting (CM-HPF vs CM-CAF β-values, Figure 2A, 2B, 2C, left panels). For the methylation analysis of miR-200a/200b/429, we surveyed the genomic region extending 5000-to-2000 bp upstream of the coding sequence recognized as the true promoter sequence (30). miR-200c and miR-141, known to be repressed by DNA methylation in prostate cancer (41), instead were already hyper-methylated in PC3 CM-HPFs (β-value: >0.8); only one cytosine of the promoter region showed a slight hyper-methylation (Figure 2D, left).

The direct involvement of DNMT3A in the observed hyper-methylation was assessed through chromatin immunoprecipitation. Analysis of the promoter region of miR-200a/200b/429, -203, -205a, and miR-200c/141 highlighted the recruitment of DNMT3A on all promoters only in CM-CAFs. DNMT1 was also recruited in CM-CAFs, with the likely function to maintain the newly deposited methylation marks (Figure 2, right panels, and Supplementary Figure 1B). Noticeably, DNMT1 was already recruited to miR-200c/141 promoter in CM-HPFs, in line with its established methylated status. A switch between DNMT3A and 3B during EMT was observed on this promoter, supporting the role of the former methyltransferase through the process (Figure 3D). DNA hyper-methylation is associated with the appearance of repressive histone modifications, H3K27me3 and H3K9me3, and/or the decrease of activating histone modifications, H3K4me3 and H3K36me3 (Figure 2, right panels), reinforcing the repressive status of these promoters.

Investigation of specific promoter regions thus shows that DNMT3A is directly involved in the regulation of miRNAs with key roles in the epithelial-to-mesenchymal transition, further highlighting and confirming the role of this DNMT in our model.

miRNome alterations in PRAD TCGA dataset patients displaying an EMT signature.

Our *ex-vivo* results on miRNome alteration were confirmed *in vivo* by analysing the PRAD TCGA dataset, crossing the miRNA expression data with the DNA methylation profile. To select for the patients displaying opposite mesenchymal phenotype, we assigned to each sample a signature: EMT-like, defined as patients presenting high expression of EMT genes and low expression of MET genes, or MET-like, displaying the opposite pattern of expression (details in materials & methods; Figure 3). Clustering the patients through this categorisation reduced their number to 87, 40 of which presented a MET profile and the remaining 47 an EMT signature. Expression and DNA methylation of the previously identified miRNAs were evaluated in our two clusters and showed a tight correlation with expression of EMT/MET factors (Figure 3).

In particular, miR-200c and miR-141 expression inversely correlates with ZEB1 (black boxed samples), in agreement with previous evidence (30), and directly correlates with GRHL2 (the regulator of ZEB1); the promoter regions of these two miRNAs are hyper-methylated in EMT compared to MET cases (red boxed samples). miR-200a, -200b and -429 display the same correlation in both expression profile and DNA methylation (when considering the true promoter region of the polycistronic pri-miRNA transcript, as for ChIP experiments), except for a cluster of cases in MET patients where we observe

methylation of the promoter and very low expression of the miRNA (red, methylation, and black, expression, boxed samples). Conversely, expression of miR-203 coherently correlates with EMT/MET genes expression, but not with the level of promoter methylation. miR-205 expression does not show a significant correlation with EMT/MET mRNA levels *in vivo*. Expression analysis also shows that DNMT3A (pan) levels do not significantly differ in the two categories, recalling the importance of the experimentally observed isoform switch during the transition between the epithelial and the mesenchymal status.

These results show that the methylation status of miRNA promoters strongly relates DNA methylation and miRNA expression of miR-200c/141 and miR-200b/200c/429 in the EMT/MET TCGA samples of prostate cancer, supporting our *in vitro* results. They also confirm the relevance of the inverse correlation between ZEB1 and miRNAs of the 200 family in EMT.

Identification of potential miRNA regulators of DNMT3A in EMT.

To further explore the mechanisms behind the regulation of DNMT3A protein levels during *ex-vivo* EMT, we examined the involvement of the miRNA-mediated regulation of *DNMT3A* mRNA. DNMT3A is a known target of various miRNAs, in particular the miR-29 family (23). We previously demonstrated that all three miRNAs of the -29 cluster (miR-29a, -29b and -29c) are down-regulated during *ex-vivo* EMT (6). Contrary to what previously assessed via qPCR, despite a reduction in read counts for miR-29a and miR-29b, their downregulation resulted not statistically significant in our RNA seq (Supplementary Figure 2A).

Therefore, we set to identify new potential DNMT3A regulators among the DE miRNAs. By enquiring multiple *in silico* tools, we produced a list of miRNAs identified by at least 2 tools that was used to isolate potential interactors of *DNMT3A* mRNA among our DE miRNAs. The analysis revealed a list of 10 up-regulated and 8 down-regulated miRNAs (Supplementary Table 2A and 2B, grey boxes). Among the down-regulated ones, our attention focused on miR-429 and miR-200b, as they are regulated by DNMT3A and contain a shared a seeding sequence directed to its 3'UTR. Conversely, among up-regulated miRNAs we noticed miR-1260a, that so far has not been linked to DNMT3A and that we previously found altered in UHRF1-silenced PC3 cells, where it resulted significantly up-regulated in combination with DNMT3A down-regulation (Supplementary Figure 2C).

Our data show that, during *ex-vivo* EMT, DNMT3A is epigenetically regulated not only via promoter methylation, as previously published (6), but potentially also by miRNome alteration, as several

deregulated miRNAs are identified by *in silico* analysis as potentially targeting *DNMT3A*-3'UTR. In particular, the down-regulated miR-200b/429 and the up-regulated miR-1260a represent the most interesting potential interactors of DNMT3A.

Validation of miR-1260a and miR-429 as regulators of *DNMT3A* mRNA and assessment of a feedback loop between miR-200b/429 and DNMT3A in EMT.

There is no current evidence in the literature about possible roles for miR-1260a or its interactors in cancer progression, while miR-200b and miR-429 have been extensively investigated (42,43). In particular, miR-200b has already been demonstrated to directly target DNMT3A in ovarian cancer (42), while the ability of miR-429 to target it is only speculated. We first assessed miR-1260a, miR-200b and miR-429 expression in our *ex-vivo* EMT model and in different PCa cell lines. We observed a significant reduction of all three miRNAs in CM-CAFs compared to CM-HPFs (Figure 4A, left panel); for miR-1260a, this result is in contrast with the RNA-seq analysis (Supplementary Table 2B). In LNCaP and PC3 non-treated cells, *DNMT3A* mRNA levels show an inverse trend with the expression of miR-1260a, miR-200b and miR-429: lower levels of *DNMT3A* mRNA and higher amounts of miRNAs were detected in LNCaP, and *vice versa* in PC3 (Figure 4A, right panel, and Supplementary Figure 2B).

Inspection of *DNMT3A*-3'UTR by accessibility analysis (37) identified two seed sites for miR-1260a and one for miR-429, shared with miR-200b (Supplementary Figure 3A). To verify the ability of these miRNAs to target *DNMT3A*-3'UTR, we co-transfected the pGL4.13-*DNMT3A*-3'UTR plasmid along with miR-1260a or miR-429 overexpressing plasmid (psiUx-miR-1260a, psiUx-miR-429) in PC3-NT cells. We did not test miR-200b as it has already been shown to target *DNMT3A* 3'UTR (42). psiUx-miR-608 and psiUx-miR-29a were used as negative and positive control, respectively, as no binding sites for miR-608 are known or predicted on *DNMT3A*-3'UTR, while miR-29a directly targets *DNMT3A*-3'UTR (23). psiUx-miR-1260a and psiUx-miR-429 reduced luciferase activity of about 40% and 30% relative to psiUx-miR-608, respectively (Figure 4B and Supplementary Figure 3C), suggesting a direct binding on *DNMT3A*-3'UTR. psiUx-miR-29a led to a 25% decrease in luciferase activity, as expected (Figure 4B). These results prove the ability of miR-429 to target DNMT3A and confirm previous data for miR-200b. To support the specificity of miR-1260a binding, we co-transfected *DNMT3A*-3'UTR deletion mutants (Δ1260a_1, Δ1260a_2 and the double mutant Δ1260a_1_2) with psiUx-miR-1260a or psiUx-miR-608. No reduction of luciferase activity was detected upon co-transfection of psiUx-miR-1260a with Δ1260a_1_2 constructs, while a reduction was observed with the Δ1260a_1 and Δ1260a_2 mutants,

separately (Supplementary Figure 3C), indicating the both sites targeted by miR-1260a contribute to its activity.

Furthermore, we characterized the effects of the over-expression/down-regulation of these miRNAs on DNMT3A levels and EMT factors. Given the statistically different (higher) levels of both miRNAs in LNCaP versus PC3, corresponding to an opposite trend in DNMT3A expression levels (Figure 4A), we performed mimicry in PC3 and inhibition in LNCaP, to evaluate the impact of the differential manipulations in the two cell lines. Both mimic-1260a and mimic-429 reduced DNMT3A mRNA and protein levels in PC3-NT, while miRNA inhibitors slightly increased them in LNCaP (Figure 4C and 4D, left). miR-429 deregulation appears to affect mostly DNMT3A1 isoform, while miR-1260a affects the two isoforms equally, and to a greater extent compared to miR-429. Since the 3'UTR is identical in both isoforms, this preference could be ascribed to secondary mechanisms linked to miR-429 variations. Concerning EMT factors (Figure 4C-4D, right panel, and Supplementary Figure 4A-4B), miR-429 had a very strong impact on all the analysed factors, in particular ZEB-1, confirming the importance of this miRNA for the transition. Conversely, the contribution of miR-1260a on EMT gene expression/protein levels resulted less evident.

Finally, we assessed whether cell growth and migration ability were also affected by the deregulation of the miRNAs. In PC3 cells, only miR-1260a mimic significantly reduced cell proliferation after five days (Figure 5A, left). Instead, miR-429 mimic strongly inhibited cell migration, with greater efficacy than miR-1260a mimic (Figure 5A, right panel). In LNCaP cells, inhibition of both miRNAs did not affect cell proliferation, while only LNA-429 mildly increased cell migration (Figure 5B, left panel). Taken together, these data argue in favour of a role of miR-429, but not of miR-1260a, on cell migration by affecting several genes involved in the epithelial-to-mesenchymal transition, rather than on cell proliferation.

Previous assessment of miR-429 and miR-200b behaviour in the PRAD patients' dataset (Figure 3) showed an inverse correlation of the expression of these miRNAs with the EMT phenotype. Conversely, miR-1260a expression was detectable only in 12 tumour samples, among which only one was present in the EMT- and MET-like clusters (Supplementary Figure 4C). miR-1260a locus methylation levels did not show any evident correlation with its expression.

In conclusion, miR-1260a can directly regulate *DNMT3A,* and its modulation significantly alters DNMT3A levels in PC3 and LNCaP cells; however, this miRNA is not abundantly expressed in prostate cancer patients and does not seem to be a direct player in the epithelial-to-mesenchymal transition.

Conversely, the feedback loop between miR-200b/-429 and DNMT3A, and the concomitant action on EMT factors such as ZEB1 underline the importance of these two miRNAs for the EMT process in PCa.

Discussion

In this study, we provide strong evidence that the interplay of DNMT3A with several miRNAs has a central role in the epithelial-to-mesenchymal transition occurring during prostate cancer progression. We identified a feedback loop between miR-429 and DNMT3A that promotes and sustains the transition towards a more mesenchymal phenotype, and we hypothesize that this is likely supported by the differential expression of two DNMT3A isoforms (a and b) during the process.

EMT is an intrinsic metastable process, susceptible to undergo the reverse Mesenchymal-to-Epithelial Transition (MET) according to the stimuli conveyed. The relevance of the molecular signals from local microenvironment and cancer-associated stroma in the induction and functional activation of the EMT and the reverse MET pathways has been greatly explored in the last decade (24,44,45); TGFβ is the most investigated player, although other factors generated from the neighbouring tumour microenvironment contribute to the process. Consistent with its inherent plasticity, it has been hypothesized that epigenetic events have crucial functions in triggering and establishing the intermediate and final phenotype. In support of this view, we previously demonstrated that reversible DNA methylation alterations are pivotal during the EMT-MET program in prostate cancer, resulting in transcriptome rewiring (6). In this context, we showed that DNMT3A induces reversible methylome changes in PC3 cells, but not in LNCaP cells, following exposure to patient-derived cancer-associated fibroblasts conditioned medium (6). We report here that microenvironmental stimuli also induce the epigenetic switches on miRNA promoters, and that DNMT3A is the putative regulator of the DNA methylation variations occurring at various miRNA promoters in our *ex vivo* model system. We especially focused on the promoter regions showing *de novo-methylation*, as we were interested in highlighting the interplay between DNMT3A and miRNAs in the transition. Indeed, miR-200c and miR-141, two of the best-known and studied miRNA regulated by DNA methylation in prostate cancer, have been reported to control DNMT3A expression (41). The chromatin immunoprecipitation data presented here confirm that DNMT3A binds to the promoter region and epigenetically regulates the miR-200 family (miR-200a/200b/429 and miR-200c/141), miR-203 and miR-205 loci. DNMT1 also binds to these promoters, suggesting its involvement in the maintenance of the newly deposited methylation on miR-

203, miR-200b/200b/429 and miR-205, while it is already present on miR-200c/141, as expected by the high DNA methylation level detected in HPF samples. Our results further highlight the role of DNMT3A in altering the expression of several onco-suppressors miRNAs, which include among others miR-639 in liver cancer cells (46) and miR-105 in gastric cancer (47).

The relevance of the epigenetic control of miRNA expression during EMT was further confirmed by analysing the miRNA database of the TCGA dataset, selecting only those samples having a clearly defined EMT/MET expression signature, and comparing the methylation profile with the miRNA expression data. In 86 evaluated patients, we detected an inverse correlation between the expression of EMT factors, such as ZEB1, and onco-suppressor miRNAs, such as miR-200c/miR-141, coupled with a strong alteration in DNA methylation, in accordance with the results from our experimental model. miR-200a/200b/429 display a strong correspondence between 5-mC levels on promoter and expression, suggesting a direct control of DNA methylation on their expression. It is worth noting that a cluster of MET-like patients, presenting an epithelial signature, show very low levels of these miRNAs. DNA methylation seems to have a relevant role in the control of miR-205 expression, but not of miR-203 *in vivo,* although miR-205, differently from our experimental setting, it is not related to the EMT/MET conditions. Altogether, our data further sustain the requirement of DNMT3A for EMT achieved by modulating the expression of a series of miRNAs involved in this process.

This study strongly supports the pivotal role of the interplay between DNMT3A and several miRNAs in EMT and, ultimately, in PCa progression**.** DNMT3A itself is a target of miRNAs; its expression, indeed, is regulated by at least miR-29 (23), miR-143 (48), and miR-200b (42). In particular, we show a feedback loop between miR-429 and DNMT3A which strongly directs cancer cells towards a more mesenchymal phenotype. While these two miRNAs have already been separately linked to EMT or DNMTs regulation in various tumours (32,42), here we assess the importance of the interplay between these factors in the transition, as well as the ability of miR-429 to directly target DNMT3A. Feedback loops between DNMT3A and miRNAs have already been demonstrated in various cancers; the DNMT3A/miR-200c loop has a relevant role during carcinogenesis and progression in gastric cancer (49), while a negative feedback between miR-143 and DNMT3A regulates cisplatin resistance in ovarian cancer (50). Altogether, these findings strongly support the idea that DNMT3A and specific miRNAs work through feedback loops to regulate important biological processes relevant to cancer, such as EMT.

miR-1260a was also identified as a novel interactor of DNMT3A potentially involved in the EMT-MET pathway. This miRNA strongly impacts DNMT3A expression, as we observed an inverse

correlation between its levels and DNMT3A expression in our *ex-vivo* model and in PCa cell lines. Its effects on the EMT factors, however, are not as prominent; our data support the hypothesis that during PCa progression the DNMT3A-miR1260a axis could be implicated in cell growth more than in the EMT process. However, investigation of the TCGA dataset resulted in the recognition of few patients expressing miR-1260a. On the basis of these data, we conclude that, despite being established as a true interactor of DNMT3A *in silico* and *in vitro*, miR-1260a is not abundantly expressed in prostate cancer patients' samples and therefore is not a fundamental player in PCa progression.

Elucidation of the complete profile of DNA methylation alterations at miRNA promoters, and the identification of feedback loops between miRNAs and DNMTs, could provide a diagnostically/prognostically significant signature for prostatic cancer patients, especially for recognising and monitoring the progression towards more aggressive traits.

Supplementary information

Supplementary figures can be found at http://carcin.oxfordjournals.org/

Funding

EPIGEN Flagship Project (EPIGEN-CNR-IT) to I.M.B., A.W. and L.S.; Italian Association for Cancer Research (IG-23068) and Regione Campania (POR Campania FESR 2014/2020, azione 1.5, CUP:B41C17000080007) to A.W.; EU H2020 MSCA-RISE project diaRNAgnosis (Grant No 101007934), Fondazione CARITRO and University of Trento, Department CIBIO to M.A.D..

Data Availability

Raw DNA methylation microarray data and raw coding RNA sequencing data have been previously deposited in the EBI ArrayExpress Database (https://www.ebi.ac.uk/arrayexpress/)(6) with accession numbers E-MTAB-4753 and E-MTAB-4752, the raw noncoding RNA sequencing data have been deposited in the EBI ArrayExpress Database with accession number E-MTAB-9835 and the Agilent microarray data are available at NCBI's Gene Expression Omnibus (GEO) (https://www.ncbi.nlm.nih.gov/geo) under accession number GSE162719.

Ethical approval

The study named “Ruolo del microambiente stromale nella immunomodulazione e nella progressione del carcinoma prostatico (Role of the stromal microenvironment for immunomodulation and for cancer progression in prostatic carcinoma)” was approved by the Ethics committee ‘Area Vasta Centro’ (Azienda Ospedaliera Universitaria Careggi, Florence, Italy) with reference number ‘BIO15.016 (26.06.2015).

Conflict of interest

All the authors declare no conflict of interest.

References

1. Ferlay, J., *et al.* (2018) Cancer incidence and mortality patterns in Europe: Estimates for 40 countries and 25 major cancers in 2018. *Eur J Cancer*.
2. Siegel, R.L., *et al.* (2018) Cancer statistics, 2018. *CA Cancer J Clin*, **68**, 7-30.
3. Angeles, A.K., *et al.* (2018) Genome-Based Classification and Therapy of Prostate Cancer. *Diagnostics (Basel)*, **8**.
4. Lo, U.G., *et al.* (2017) The Role and Mechanism of Epithelial-to-Mesenchymal Transition in Prostate Cancer Progression. *Int J Mol Sci*, **18**.
5. Nieto, M.A., *et al.* (2016) EMT: 2016. *Cell*, **166**, 21-45.
6. Pistore, C., *et al.* (2017) DNA methylation variations are required for epithelial-to-mesenchymal transition induced by cancer-associated fibroblasts in prostate cancer cells. *Oncogene*, **36**, 5551-5566.
7. Baylin, S.B., *et al.* (2011) A decade of exploring the cancer epigenome - biological and translational implications. *Nat Rev Cancer*, **11**, 726-34.
8. Heyn, H., *et al.* (2012) DNA methylation profiling in the clinic: applications and challenges. *Nat Rev Genet*, **13**, 679-92.
9. Paziewska, A., *et al.* (2014) DNA methylation status is more reliable than gene expression at detecting cancer in prostate biopsy. *Br J Cancer*, **111**, 781-9.
10. Ashraf, W., *et al.* (2017) The epigenetic integrator UHRF1: on the road to become a universal biomarker for cancer. *Oncotarget*, **8**, 51946-51962.
11. Angulo, J.C., *et al.* (2016) Development of Castration Resistant Prostate Cancer can be Predicted by a DNA Hypermethylation Profile. *J Urol*, **195**, 619-26.
12. Ellinger, J., *et al.* (2008) CpG island hypermethylation at multiple gene sites in diagnosis and prognosis of prostate cancer. *Urology*, **71**, 161-7.
13. Massie, C.E., *et al.* (2017) The importance of DNA methylation in prostate cancer development. *J Steroid Biochem Mol Biol*, **166**, 1-15.
14. Qin, W., *et al.* (2015) DNA methylation requires a DNMT1 ubiquitin interacting motif (UIM) and histone ubiquitination. *Cell Res*, **25**, 911-29.
15. Lyko, F. (2018) The DNA methyltransferase family: a versatile toolkit for epigenetic regulation. *Nat Rev Genet*, **19**, 81-92.
16. Lin, R.K., *et al.* (2014) Dysregulated transcriptional and post-translational control of DNA methyltransferases in cancer. *Cell Biosci*, **4**, 46.
17. Gravina, G.L., *et al.* (2013) Increased levels of DNA methyltransferases are associated with the tumorigenic capacity of prostate cancer cells. *Oncol Rep*, **29**, 1189-95.
18. Gravina, G.L., *et al.* (2011) Hormonal therapy promotes hormone-resistant phenotype by increasing DNMT activity and expression in prostate cancer models. *Endocrinology*, **152**, 4550-61.
19. Wahid, F., *et al.* (2010) MicroRNAs: synthesis, mechanism, function, and recent clinical trials. *Biochim Biophys Acta*, **1803**, 1231-43.

20. Peng, Y., *et al.* (2016) The role of MicroRNAs in human cancer. *Signal Transduct Target Ther*, **1**, 15004.
21. Sharma, N., *et al.* (2018) The microRNA signatures: aberrantly expressed miRNAs in prostate cancer. *Clin Transl Oncol*.
22. Bryzgunova, O.E., *et al.* (2018) MicroRNA-guided gene expression in prostate cancer: Literature and database overview. *J Gene Med*, **20**, e3016.
23. Morita, S., *et al.* (2013) miR-29 represses the activities of DNA methyltransferases and DNA demethylases. *Int J Mol Sci*, **14**, 14647-58.
24. Davalos, V., *et al.* (2012) Dynamic epigenetic regulation of the microRNA-200 family mediates epithelial and mesenchymal transitions in human tumorigenesis. *Oncogene*, **31**, 2062-74.
25. Lin, S., *et al.* (2015) MicroRNA biogenesis pathways in cancer. *Nat Rev Cancer*, **15**, 321-33.
26. Ramassone, A., *et al.* (2018) Epigenetics and MicroRNAs in Cancer. *Int J Mol Sci*, **19**.
27. Saini, S., *et al.* (2011) Regulatory Role of mir-203 in Prostate Cancer Progression and Metastasis. *Clin Cancer Res*, **17**, 5287-98.
28. Kalogirou, C., *et al.* (2013) MiR-205 is progressively down-regulated in lymph node metastasis but fails as a prognostic biomarker in high-risk prostate cancer. *Int J Mol Sci*, **14**, 21414-34.
29. Ru, P., *et al.* (2012) miRNA-29b suppresses prostate cancer metastasis by regulating epithelial-mesenchymal transition signaling. *Mol Cancer Ther*, **11**, 1166-73.
30. Pieraccioli, M., *et al.* (2013) Activation of miR200 by c-Myb depends on ZEB1 expression and miR200 promoter methylation. *Cell Cycle*, **12**, 2309-20.
31. Bracken, C.P., *et al.* (2008) A double-negative feedback loop between ZEB1-SIP1 and the microRNA-200 family regulates epithelial-mesenchymal transition. *Cancer Res*, **68**, 7846-54.
32. Gregory, P.A., *et al.* (2008) The miR-200 family and miR-205 regulate epithelial to mesenchymal transition by targeting ZEB1 and SIP1. *Nat Cell Biol*, **10**, 593-601.
33. Chen, Y., *et al.* (2020) miRDB: an online database for prediction of functional microRNA targets. *Nucleic Acids Res*, **48**, D127-D131.
34. Agarwal, V., *et al.* (2015) Predicting effective microRNA target sites in mammalian mRNAs. *Elife*, **4**.
35. Oulas, A., *et al.* (2012) A new microRNA target prediction tool identifies a novel interaction of a putative miRNA with CCND2. *RNA Biol*, **9**, 1196-207.
36. Pio, G., *et al.* (2015) ComiRNet: a web-based system for the analysis of miRNA-gene regulatory networks. *BMC Bioinformatics*, **16 Suppl 9**, S7.
37. Kertesz, M., *et al.* (2007) The role of site accessibility in microRNA target recognition. *Nat Genet*, **39**, 1278-84.
38. Rehmsmeier, M., *et al.* (2004) Fast and effective prediction of microRNA/target duplexes. *RNA*, **10**, 1507-17.
39. Denti, M.A., *et al.* (2004) A new vector, based on the PolII promoter of the U1 snRNA gene, for the expression of siRNAs in mammalian cells. *Mol Ther*, **10**, 191-9.
40. Fang, H., *et al.* (2009) ArrayTrack: an FDA and public genomic tool. *Methods Mol Biol*, **563**, 379-98.
41. Lynch, S.M., *et al.* (2016) Regulation of miR-200c and miR-141 by Methylation in Prostate Cancer. *Prostate*, **76**, 1146-59.
42. Liu, J., *et al.* (2019) miR-200b and miR-200c co-contribute to the cisplatin sensitivity of ovarian cancer cells by targeting DNA methyltransferases. *Oncol Lett*, **17**, 1453-1460.
43. Guo, C.M., *et al.* (2020) miR-429 as biomarker for diagnosis, treatment and prognosis of cancers and its potential action mechanisms: A systematic literature review. *Neoplasma*, **67**, 215-228.
44. Pardali, K., *et al.* (2007) Actions of TGF-beta as tumor suppressor and pro-metastatic factor in human cancer. *Biochim Biophys Acta*, **1775**, 21-62.
45. Xu, J., *et al.* (2009) TGF-beta-induced epithelial to mesenchymal transition. *Cell Res*, **19**, 156-72.
46. Xiao, J., *et al.* (2020) miR-639 Expression Is Silenced by DNMT3A-Mediated Hypermethylation and Functions as a Tumor Suppressor in Liver Cancer Cells. *Mol Ther*, **28**, 587-598.
47. Zhou, G.Q., *et al.* (2017) DNMT3A-mediated down-regulation of microRNA-105 promotes gastric cancer cell proliferation. *Eur Rev Med Pharmacol Sci*, **21**, 3377-3383.
48. Karimi, L., *et al.* (2017) Function of microRNA-143 in different signal pathways in cancer: New insights into cancer therapy. *Biomed Pharmacother*, **91**, 121-131.
49. Li, Y., *et al.* (2016) Epigenetically deregulated miR-200c is involved in a negative feedback loop with DNMT3a in gastric cancer cells. *Oncol Rep*, **36**, 2108-16.
50. Han, X., *et al.* (2021) The negative feedback between miR-143 and DNMT3A regulates cisplatin resistance in ovarian cancer. *Cell Biol Int*, **45**, 227-237.

Legends to Figures

Figure 1. Analysis of DNMT3A variants and miRNAs transcription/DNA methylation profiling during *ex-vivo* EMT. (A) Alteration of mRNA and protein levels of DNMT3A variants following EMT induction. DNMT3A variant 1 (DNMT3A1, isoform a) and variant 2 (DNMT3A2, isoform b) were analysed by qPCR (together with DNMT3A pan, assessing all known variants) and Western Blot in CM-HPFs and CM-CAFs PC3 cells. (6). **(B-C) Alteration of miRNA transcription profile following EMT induction.** Heatmap **(B)** and volcano plot **(C)** of the RNA-Seq analysis (P_adj $\leqslant$0.05 and FC $\geqslant$1.5; $\leqslant$-1.5) of miRNAs during EMT (CM-CAFs vs CM-HPFs). The results presented in B are the average of three independent biological experiments. The P_adj value is computed performing the Benjamini–Hochberg test. **(D) Alteration of miRNA promoter methylation following EMT induction.** The scatter plot shows the distribution during EMT of hyper-methylated (Δβ-value $\geqslant$0.2; lower triangle) and hypo-methylated (Δβ-value $\leqslant$–0.2; upper triangle) cytosines of the DE and DM miRNAs. The scatter plot is subdivided into four gates (G1, G2, G3 and G4). G1: cytosines strongly hypo-methylated, up to complete demethylation (β-values not exceeding 0.2 in CM-CAFs); G2: hypo-methylated cytosines that achieved β-values >0.2 in CM-CAFs; G3: hyper-methylated cytosines with β-values >0.2 in CM-HPFs; G4: nearly un-methylated cytosines becoming hyper- or *de novo* methylated during EMT. The differentially methylated up- (upper part) and down- (lower part) regulated miRNAs are shown separately. On the right, box plots of the cytosine methylation variations during EMT in DE and DM miRNAs. G1+G2: All hypo-methylated cytosines'; G1: G1-gated cytosines; G2: G2 gated cytosines; G3+G4: all hyper-methylated cytosines; G3: G3-gated cytosines. The P-value is calculated by Mann–Whitney U-test.

Figure 2. Analysis of DNMT3A recruitment to specific miRNA promoters during *ex-vivo* EMT. (A-D, left) miRNA promoter structure and cytosine methylation analysis. Methylation levels were obtained through Illumina 450k array, as previously shown: miR-203 **(A)** miR-200b/200a/429 **(B)** miR-205a **(C)** and miR-200c/141 **(D)** promoter status was evaluated after exposure to CM-HPFs and CM-CAFs. The position of the different analysed cytosines is reported in the cartoons of the four promoter regions, together with the related sites analysed by ChIP. Nucleotide number and position on the chromosomes refer to the reference GRCh37.p13 primary assembly (annotation release 105.20201022). (**A-D, right**) **Evaluation of the epigenetic status of miRNA promoters.** mir-203 **(A)**,

miR-200a/200b/429 **(B)** miR-205a **(C)** and miR-200c/141 **(D)** promoters were investigated through ChIP experiments performed against DNA methyltransferases (DNMT1, -3A and -3B) and the indicated histone modifications (H3K9me3, H3K27me3, H3K4me3 and H3K36me3). Bars show Mean ± SD of three technical replicates of three independent experiments (unpaired Student's t test).

Figure 3. Alteration of the miRNome in prostate cancer patients (PRAD TCGA data set). A primary prostate adenocarcinoma (TCGA-PRAD) dataset containing 494 patients was enquired (https://gdc-portal.nci.nih.gov). IlluminaHiSeq mRNA-Seq expression data were used to classify patients; each patient was assigned to the EMT-like category when EMT genes were expressed at high levels (>Q3, or Q4) and MET genes at low levels (<Q1or Q2), or to the MET-like category when displaying the opposite signature (see material and methods). Patients showing positive scores for EMT- or MET-like profiles were chosen (47 and 40 cases, respectively); the heatmap shows the expression of the EMT genes and of DNMTs (IlluminaHiSeq), and the comparison between miRNA expression (IlluminaHiSeq) and cytosines DNA methylation (Illumina Infinium, HumanMethylation 450 array) of the miRNAs found differentially expressed and methylated in CM-CAFs vs CM-HFPs PC3 cells (Black/red boxes: Expression/methylation of miRNAs; Arrows: Expression of ZEB1 and DNMT3A).

Figure 4. Identification and validation of new potential *DNMT3A* regulators among miRNAs altered during *ex-vivo* EMT. (A) Evaluation of miR-200b, miR-429 and miR-1260a expression levels during EMT and in PCa cell lines. Transcriptional levels of the three miRNAs were assessed in CM-CAFs vs CM-HPFs PC3 cells and in LNCaP vs PC3-NT (non-treated) cells. miRNA expression was compared to DNMT3A (pan) expression levels in the same cells. **(B) Functional analysis of miR-429 and miR-1260a binding to *DNMT3A* 3'UTR.** *DNMT3A*-3'UTR was cloned downstream of the Firefly luciferase gene in pGL4.13 plasmid and co-transfected in PC3-NT cells with plasmids overexpressing miR-429 or miR-1260a. miR-608 was used as negative control, miR-29a/b as positive control. Empty = transfected with psiUx-empty; Non-Transf = non-transfected cells (*DNMT3A*-3'UTR only). (N=3; Student's t test). **(C-D) Characterization of miR-429 and miR-1260a overexpression/down-regulation in prostate cancer cell lines. (Left)** DNMT3A variations in PC3-NT cells transfected with MIMIC oligos **(C)** and in LNCaP cells transfected with LNA-inhibitor oligos **(C)** were evaluated both at mRNA and protein levels. **(Right)** Alteration of the transcriptional and protein levels of key EMT factors was evaluated following miR-429 /miR-1260a mimicry in PC3-NT cells and miR-429 /miR-1260a inhibition in LNCaP cells. n.d.= not detected. (N=4; Student's t test).

Figure 5. Phenotypic alterations following miR-429 or miR-1260a overexpression /down-regulation. (A) Proliferation and migration ability of PC3-NT cells after miR-429 or miR-1260a ectopic expression. Cell growth curve (left), and wound healing assays (right) after mimics transfection. **(B) Proliferation and migration of LNCaP cells after inhibition of miR-429 or miR-1260a.** Cell growth curve (left) and wound healing assays (right) after LNA-inhibitors transfection. Pictures were taken at T0, 24 hours and 48 hours after monolayer wounding; cell growth was assessed at the same time points. Cell migration is shown as means values ± SDs of the measurements of the cell-free area for each time point and condition. Each experiment was performed in triplicate. (One-Way ANOVA test). Pictures shown are representative of the average behaviour.

Figure 1

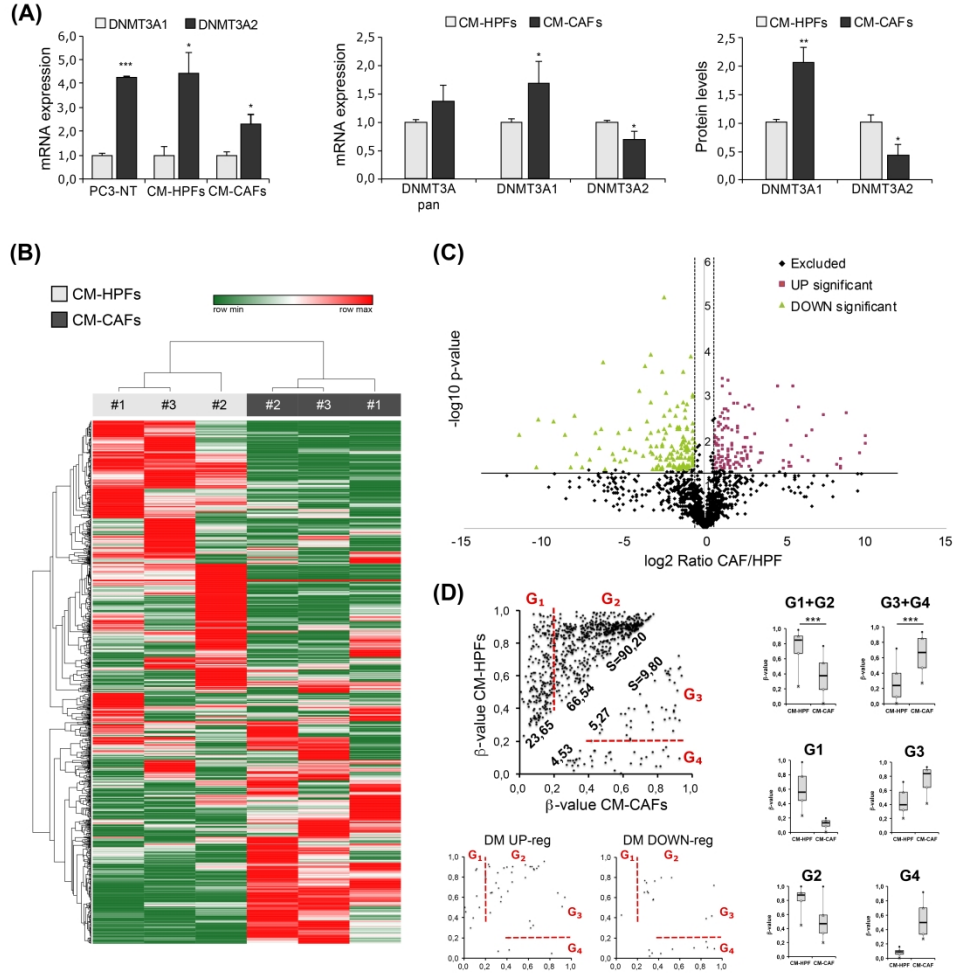

Figure 1. Analysis of DNMT3A variants and miRNAs transcription/DNA methylation profiling during ex-vivo EMT. (A) Alteration of mRNA and protein levels of DNMT3A variants following EMT induction. DNMT3A variant 1 (DNMT3A1, isoform a) and variant 2 (DNMT3A2, isoform b) were analysed by qPCR (together with DNMT3A pan, assessing all known variants) and Western Blot in CM-HPFs and CM-CAFs PC3 cells. (6). (B-C) Alteration of miRNA transcription profile following EMT induction. Heatmap (B) and volcano plot (C) of the RNA-Seq analysis (P_adj ⩽0.05 and log2 FC ⩾1.5; ⩽-1.5) of miRNAs during EMT (CM-CAFs vs CM-HPFs). The results presented in B are the average of three independent biological experiments. The P_adj value is computed performing the Benjamini–Hochberg test. (D) Alteration of miRNA promoter methylation following EMT induction. The scatter plot shows the distribution during EMT of hyper-methylated (Δβ-value ⩾0.2; lower triangle) and hypo-methylated (Δβ-value ⩽–0.2; upper triangle) cytosines of the DE and DM miRNAs. The scatter plot is subdivided into four gates (G1, G2, G3 and G4). G1: cytosines strongly hypo-methylated, up to complete demethylation (β-values not exceeding 0.2 in CM-CAFs); G2: hypo-methylated cytosines that achieved β-values >0.2 in CM-CAFs; G3: hyper-methylated cytosines with β-values >0.2 in CM-HPFs; G4: nearly un-methylated cytosines becoming hyper- or de novo methylated during EMT. The differentially methylated up- (upper part) and down- (lower part) regulated miRNAs are shown separately. On the right, box plots of the cytosine methylation variations during EMT in DE and DM miRNAs. G1+G2: All hypo-methylated cytosines'; G1: G1-gated cytosines; G2: G2 gated cytosines; G3+G4: all hyper-methylated cytosines; G3: G3-gated cytosines. The P-value is calculated by Mann–Whitney U-test.

Figure 2

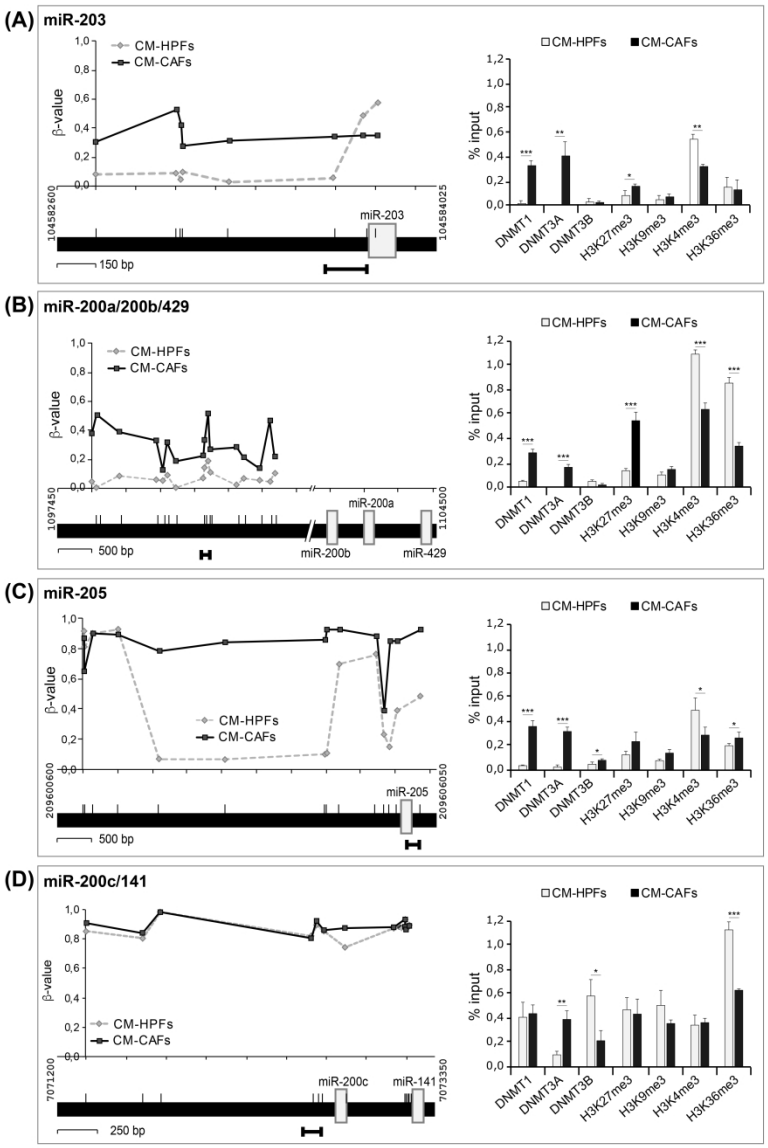

Figure 2. Analysis of DNMT3A recruitment to specific miRNA promoters during ex-vivo EMT. (A-D, left) miRNA promoter structure and cytosine methylation analysis. Methylation levels were obtained through Illumina 450k array, as previously shown: miR-203 (A) miR-200b/200a/429 (B) miR-205a (C) and miR-200c/141 (D) promoter status was evaluated after exposure to CM-HPFs and CM-CAFs. The position of the different analysed cytosines is reported in the cartoons of the four promoter regions, together with the related sites analysed by ChIP. Nucleotide number and position on the chromosomes refer to the reference GRCh37.p13 primary assembly (annotation release 105.20201022). (A-D, right) Evaluation of the epigenetic status of miRNA promoters. mir-203 (A), miR-200a/200b/429 (B) miR-205a (C) and miR-200c/141 (D) promoters were investigated through ChIP experiments performed against DNA methyltransferases (DNMT1, -3A and -3B) and the indicated histone modifications (H3K9me3, H3K27me3, H3K4me3 and H3K36me3). Bars show Mean ± SD of three technical replicates of three independent experiments (unpaired Student's t test).

Figure 3

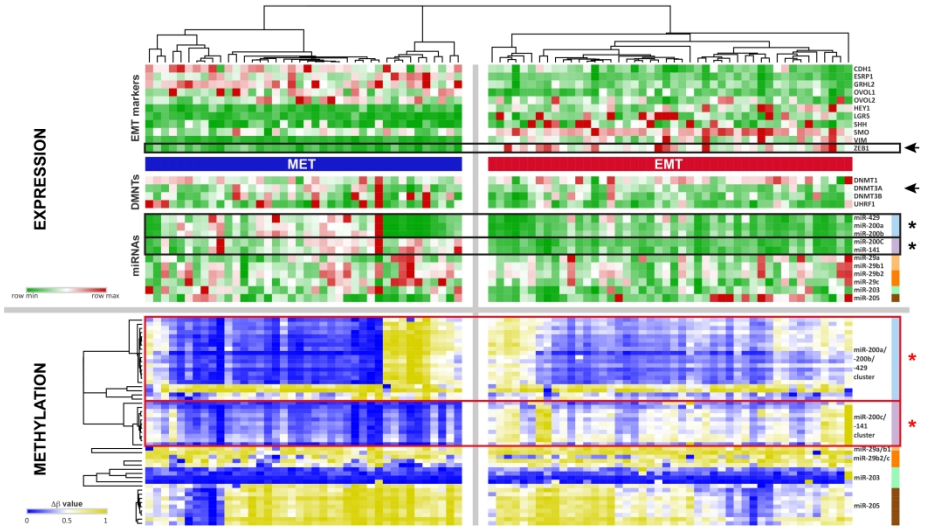

Figure 3. Alteration of the miRNome in prostate cancer patients (PRAD TCGA data set). A primary prostate adenocarcinoma (TCGA-PRAD) dataset containing 494 patients was enquired (https://gdc-portal.nci.nih.gov). IlluminaHiSeq mRNA-Seq expression data were used to classify patients; each patient was assigned to the EMT-like category when EMT genes were expressed at high levels (>Q3, or Q4) and MET genes at low levels (<Q1or Q2), or to the MET-like category when displaying the opposite signature (see material and methods). Patients showing positive scores for EMT- or MET-like profiles were chosen (47 and 40 cases, respectively); the heatmap shows the expression of the EMT genes and of DNMTs (IlluminaHiSeq), and the comparison between miRNA expression (IlluminaHiSeq) and cytosines DNA methylation (Illumina Infinium, HumanMethylation 450 array) of the miRNAs found differentially expressed and methylated in CM-CAFs vs CM-HFPs PC3 cells (Black/red boxes: Expression/methylation of miRNAs; Arrows: Expression of ZEB1 and DNMT3A).

Figure 4

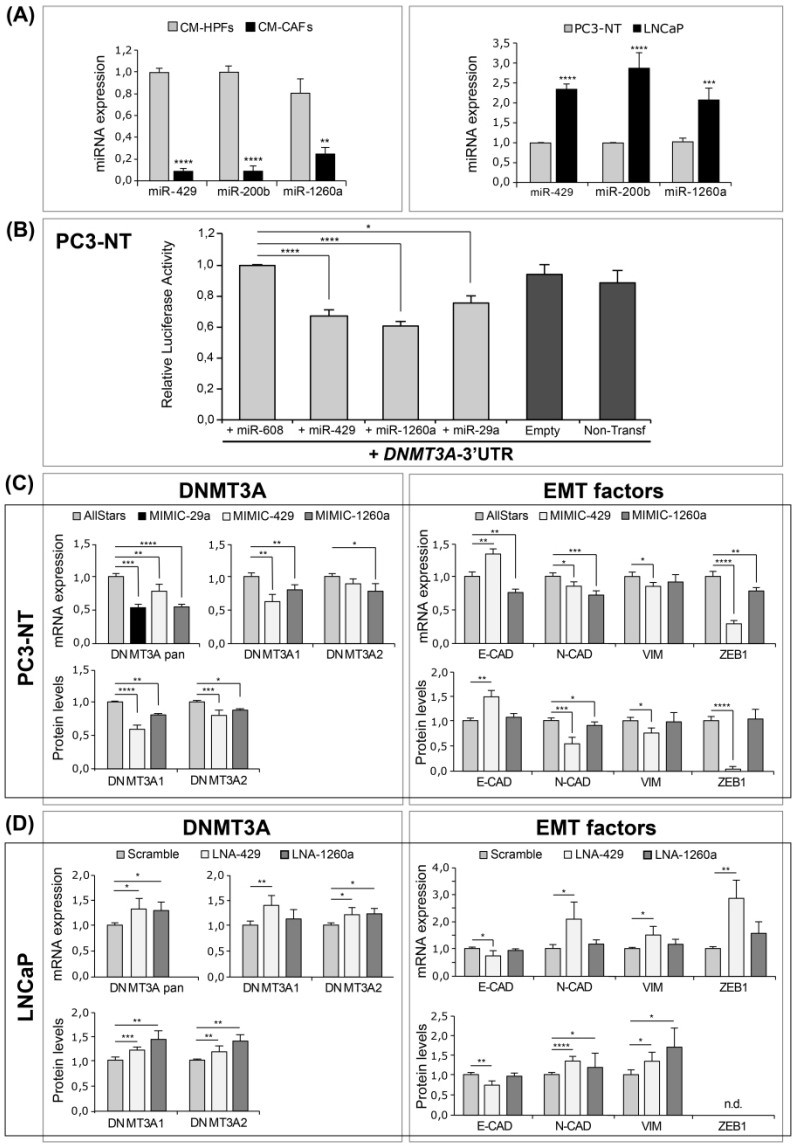

Figure 4. Identification and validation of new potential DNMT3A regulators among miRNAs altered during ex-vivo EMT. (A) Evaluation of miR-200b, miR-429 and miR-1260a expression levels during EMT and in PCa cell lines. Transcriptional levels of the three miRNAs were assessed in CM-CAFs vs CM-HPFs PC3 cells and in LNCaP vs PC3-NT (non-treated) cells. miRNA expression was compared to DNMT3A (pan) expression levels in the same cells. (B) Functional analysis of miR-429 and miR-1260a binding to DNMT3A 3'UTR. DNMT3A-3'UTR was cloned downstream of the Firefly luciferase gene in pGL4.13 plasmid and co-transfected in PC3-NT cells with plasmids overexpressing miR-429 or miR-1260a. miR-608 was used as negative control, miR-29a/b as positive control. Empty = transfected with psiUx-empty; Non-Transf = non-transfected cells (DNMT3A-3'UTR only). (N=3; Student's t test). (C-D) Characterization of miR-429 and miR-1260a overexpression/down-regulation in prostate cancer cell lines. (Left) DNMT3A variations in PC3-NT cells transfected with MIMIC oligos (C) and in LNCaP cells transfected with LNA-inhibitor oligos (C) were evaluated both at mRNA and protein levels. (Right) Alteration of the transcriptional and protein levels of key EMT factors was evaluated following miR-429 /miR-1260a mimicry in PC3-NT cells and miR-429 /miR-1260a inhibition in LNCaP cells. n.d. = not detected. (N=4; Student's t test).

Figure 5

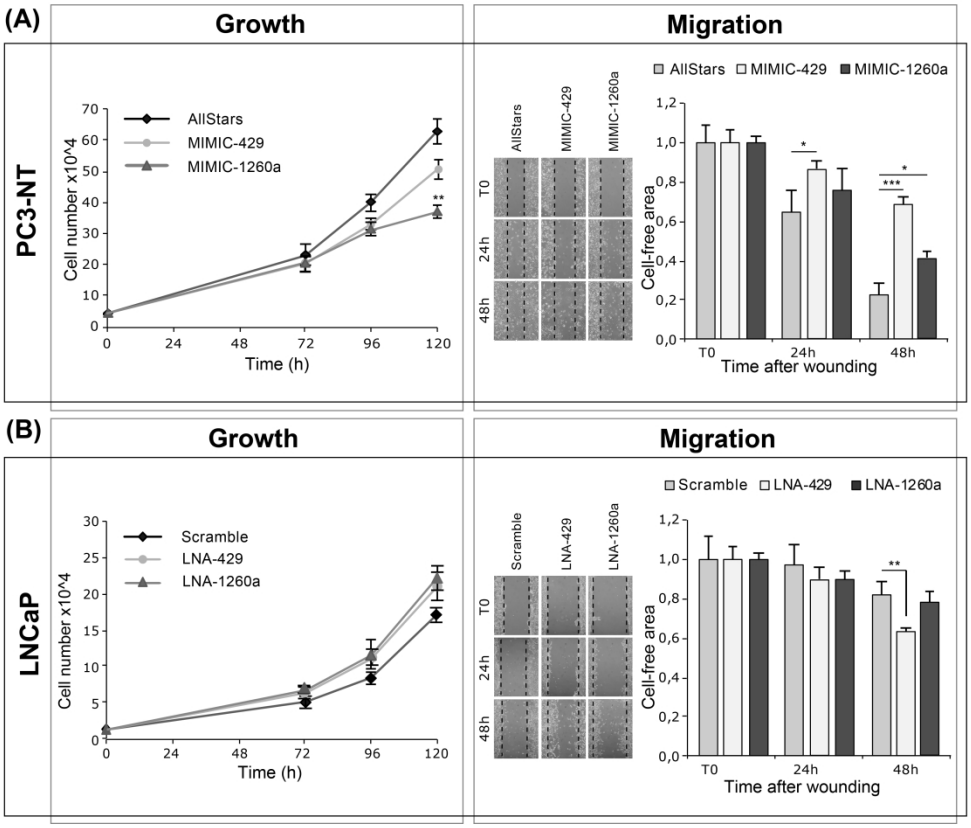

Figure 5. Phenotypic alterations following miR-429 or miR-1260a overexpression /down-regulation. (A) Proliferation and migration ability of PC3-NT cells after miR-429 or miR-1260a ectopic expression. Cell growth curve (left), and wound healing assays (right) after mimics transfection. (B) Proliferation and migration of LNCaP cells after inhibition of miR-429 or miR-1260a. Cell growth curve (left) and wound healing assays (right) after LNA-inhibitors transfection. Pictures were taken at T0, 24 hours and 48 hours after monolayer wounding; cell growth was assessed at the same time points. Cell migration is shown as means values ± SDs of the measurements of the cell-free area for each time point and condition. Each experiment was performed in triplicate. (One-Way ANOVA test). Pictures shown are representative of the average behaviour.

1A. Primer sequences (Expression and cloning)		
GAPDH	For	5'-TTGATTTTGGAGGGATCTCG-3'
	Rev	5'-GAGTCAACGGATTTGGTCGT-3'
DNMT3A pan	For	5'-CTCGAGTCCAACCCTGTGAT-3'
	Rev	5'-CTTTGCCCTGCTTTATGGAG-3'
DNMT3A1	For	5'-GTCACACGCCAAAGGACC-3'
	Rev	5'-GCTGCACCCTCTCCCTCT-3'
DNMT3A2	For	5'-CCAAGACGGGCAGCTACT-3'
	Rev	5'-ATCACACTCGTCTTTCAGGC-3'
CDH1	For	5'-ATGAGTGTCCCCCGGTATCTTC-3'
	Rev	5'-ACGAGCAGAAGAATCATAAGGCG-3'
N-CAD	For	5'-GCAGAGACTTGCGAAACTCC-3'
	Rev	5'-CACCATTAAGCCGAGTGATGG-3'
VIM	For	5'-GAGTCCACTGAGTACCGGAG-3'
	Rev	5'-ACGAGCCATTTCCTCCTTCA-3'
ZEB-1	For	5'-CTGATTCCCCAGGTGGCATA-3'
	Rev	5'-GGGCGGTGTAGAATCAGAGT-3'
miR-429	For	5'-ACTGAGATCTTGCAGGGAACCTTTGCCAAG-3'
	Rev	5'-ACTG***CTCGAG***GGCCCCA-3'
miR-1260a	For	5'-ATCGAGATCTTGGGATTCCACCAAGAAGGC-3'
	Rev	5'-ATCG***CTCGAG***TGGCCTGTATCTGTTGTAGC-3'
miR-608	For	5'-ACTGAGATCTGGTAATGGCTCCATCTGGAG-3'
	Rev	5'-ACTG***CTCGAG***TTGCAGACTCTTGGGCCCTT-3'
miR-29a	For	5'ACTGAGATCTCAGAGACTTGAGCATC-3'
	Rev	5'-ACTG***CTCGAG***AGTGTTTCTAGGTATC-3'
Delta_1260_1	For	5'-CAATACCTTGCAGAGGAAGAGAGGAAAAAAGG-3'
	Rev	5'-CCTTTTTTCCTCTCTTCCTCTGCAAGGTATTG-3'
Delta_1260_2	For	5'-GGGCTCCTTGTCAGAACTAATGGCC-3'
	Rev	5'-GGCCATTAGTTCTGACAAGGAGCCC-3'

1B. Primer sequences (ChIP)		
miR-203	For	5'-CGTCTAAGGCGTCCGGTA-3'
	Rev	5'-GAGCTGCGGAGAGAGGAG-3'
miR-200a/b/-429	For	5'-TAATTAACCCCCCGGGAG-3'
	Rev	5'-AATGTGCTGCCAACCATGC-3'
miR-205	For	5'-CCTGCAGTGTCTCTCCAACT-3'
	Rev	5'-CCACCTCTCAGAACCCACAC-3'
miR-200c/141	For	5'-GTAGGGGAAGGTGGCTCAGA-3'
	Rev	5'-GGGGACACTTCCTGGTGA-3'

Supplementary Table 1. PCR primers used in the study. 1A. PCR primers were designed to evaluate the expression of mRNA transcripts. Primes for cloning and to perform mutagenesis of miR1260a (in two different sites) are also listed in 1A. Underlined: BglII restriction site; ***Italics Bold***: XhoI restriction site. **1B.** PCR primers for ChIP were designed in the promoter region of the investigated miRNAs (see Figure 2 for specific sites).

2A. SIGNIFICANTLY UP-REGULATED miRNAS

135 miRNA showed fold change >1.5 and p-value <0.05

miRNA	Log Ratio	t test
hsa-miR-551b-5p	10,06	0,014
hsa-miR-509-3p	10,02	0,010
hsa-miR-6744-5p	9,66	0,022
hsa-miR-551b-3p	8,81	0,003
hsa-miR-1267	**8,52**	**0,049**
hsa-miR-126-5p	8,51	0,044
hsa-miR-126-3p	8,44	0,029
hsa-miR-508-3p	8,19	0,041
hsa-miR-892b	7,41	0,003
hsa-miR-3065-5p	**6,71**	**0,007**
hsa-miR-4421	6,50	0,033
hsa-miR-10b-5p	6,30	0,009
hsa-miR-522-3p	6,11	0,028
hsa-miR-3065-3p	5,92	0,002
hsa-miR-708-3p	5,54	0,001
hsa-miR-3185	5,54	0,001
hsa-miR-10b-3p	5,45	0,043
hsa-miR-6500-3p	5,36	0,015
hsa-miR-4636	5,29	0,046
hsa-miR-509-5p	**5,29**	**0,046**
hsa-miR-138-1-3p	5,27	0,035
hsa-miR-6501-3p	5,27	0,035
hsa-miR-514a-3p	5,15	0,004
hsa-miR-3189-5p	4,94	0,049
hsa-miR-1287-3p	4,94	0,049
hsa-miR-153-5p	4,88	0,033
hsa-miR-6833-5p	**4,54**	**0,001**
hsa-miR-4497	4,54	0,001
hsa-miR-6757-3p	4,54	0,001
hsa-miR-210-5p	3,59	0,023
hsa-miR-616-3p	3,55	0,033
hsa-miR-199b-5p	3,52	0,022
hsa-miR-5699-5p	3,39	0,037
hsa-miR-873-3p	3,15	0,009
hsa-miR-3129-3p	2,99	0,002
hsa-miR-1269a	2,91	0,021
hsa-miR-4795-3p	2,88	0,016
hsa-miR-210-3p	2,81	0,002
hsa-miR-143-3p	2,80	0,043
hsa-miR-140-5p	2,69	0,030
hsa-miR-6892-3p	2,68	0,030
hsa-miR-486-5p	2,67	0,027
hsa-miR-580-5p	2,67	0,026
hsa-miR-873-5p	2,65	0,010
hsa-miR-6784-3p	2,61	0,010
hsa-miR-4731-3p	2,59	0,016
hsa-miR-6892-5p	2,59	0,002
hsa-miR-516a-5p	2,55	0,021
hsa-miR-3622a-5p	**2,46**	**0,030**
hsa-miR-3614-5p	2,39	0,017
hsa-miR-6875-5p	2,37	0,033
hsa-miR-653-5p	2,37	0,033
hsa-miR-455-3p	2,32	0,046
hsa-miR-628-5p	2,31	0,031
hsa-miR-643	2,28	0,023
hsa-miR-95-3p	2,21	0,040
hsa-miR-345-5p	2,11	0,006
hsa-miR-6501-5p	2,07	0,036
hsa-miR-140-3p	2,05	0,023
hsa-miR-582-5p	2,04	0,006
hsa-miR-6833-3p	2,04	0,008
hsa-miR-582-3p	2,03	0,002
hsa-miR-874-5p	2,01	0,028
hsa-miR-455-5p	1,98	0,036
hsa-miR-3605-3p	1,91	0,027
hsa-miR-2116-5p	1,91	0,050
hsa-miR-6871-5p	1,87	0,042
hsa-miR-328-3p	1,85	0,002
hsa-miR-3605-5p	1,77	0,018
hsa-miR-191-5p	1,75	0,015
hsa-miR-616-5p	1,75	0,007
hsa-miR-345-3p	1,67	0,014
hsa-miR-625-3p	1,66	0,032
hsa-miR-2116-3p	1,64	0,049
hsa-miR-188-3p	**1,61**	**0,046**
hsa-let-7b-3p	1,56	0,001
hsa-miR-500a-3p	1,54	0,001
hsa-miR-4454	1,52	0,028
hsa-miR-3934-5p	1,51	0,001
hsa-miR-574-3p	1,50	0,004
hsa-miR-671-3p	1,49	0,006
hsa-miR-152-3p	1,47	0,033
hsa-miR-1260a	**1,46**	**0,041**
hsa-miR-6791-3p	1,44	0,024
hsa-miR-584-5p	1,44	0,038
hsa-miR-502-3p	**1,43**	**0,003**
hsa-miR-3129-5p	**1,43**	**0,018**
hsa-miR-196b-5p	1,43	0,021
hsa-miR-627-5p	1,35	0,002
hsa-miR-625-5p	1,34	0,006
hsa-let-7f-2-3p	1,33	0,029
hsa-miR-330-3p	1,29	0,006
hsa-miR-425-3p	1,27	0,004
hsa-miR-181c-3p	1,26	0,002
hsa-miR-627-3p	1,25	0,048
hsa-miR-660-5p	1,24	0,039
hsa-miR-501-3p	**1,21**	**0,050**
hsa-miR-26a-5p	1,19	0,043
hsa-miR-3182	1,19	0,050
hsa-miR-1908-5p	1,18	0,018
hsa-miR-500a-5p	1,16	0,033
hsa-miR-92b-3p	1,13	0,010
hsa-miR-130b-5p	1,13	0,007
hsa-miR-28-3p	1,11	0,000
hsa-miR-671-5p	1,10	0,028
hsa-miR-425-5p	1,09	0,003
hsa-miR-182-5p	1,08	0,001
hsa-miR-125b-1-3p	1,08	0,015
hsa-miR-502-5p	1,06	0,047
hsa-miR-26b-3p	1,02	0,005
hsa-miR-766-5p	1,02	0,035
hsa-let-7i-5p	1,02	0,004
hsa-miR-186-5p	0,99	0,026
hsa-miR-1976	0,95	0,027
hsa-miR-23b-3p	0,94	0,024
hsa-miR-550a-5p	0,94	0,012
hsa-miR-100-5p	0,93	0,015
hsa-miR-100-3p	0,86	0,020
hsa-miR-191-3p	0,85	0,031
hsa-miR-125b-5p	0,85	0,006
hsa-miR-181c-5p	0,84	0,005
hsa-let-7i-3p	0,82	0,014
hsa-miR-27b-5p	0,77	0,015
hsa-miR-26b-5p	0,76	0,048
hsa-miR-183-5p	0,74	0,036
hsa-miR-629-5p	0,71	0,030
hsa-miR-3661	0,67	0,027
hsa-miR-589-5p	0,66	0,013
hsa-miR-149-5p	0,66	0,013
hsa-miR-21-3p	0,65	0,009
hsa-miR-589-3p	0,65	0,041
hsa-miR-561-5p	0,64	0,010
hsa-miR-301a-3p	0,63	0,050
hsa-miR-548l	0,61	0,007
hsa-miR-548e-5p	0,60	0,041

Supplementary Table 2A. List of up-regulated miRNAs. miRNA expression profile significantly differs in PC3 exposed for 3 days to CM-CAFs compared to CM-HPFs. Fold change (FC) variations ⩾1.5 and ⩽−1.5 of the differentially expressed (DE) miRNAs were used to define up- and down-regulated miRNAs, respectively. Out of the 1276 deregulated miRNAs, 302 showed a p-value <0.05; 135 miRNAs showed log2 Ratio ⩾ 0.6 (fold change ⩾ 1.5). Grey boxes indicate miRNAs predicted to target DNMT3A.

2B. SIGNIFICANTLY DOWN-REGULATED miRNAS

149 miRNA showed fold change <-1.5 and p-value <0.05

miRNA	Log Ratio	t test
hsa-miR-3944-3p	-11,61	0,008
hsa-miR-30a-5p	**-10,47**	**0,045**
hsa-miR-30a-3p	-10,33	0,004
hsa-miR-4326	-9,46	0,004
hsa-let-7d-3p	-8,73	0,008
hsa-miR-7706	-8,40	0,045
hsa-miR-1276	-8,09	0,003
hsa-miR-324-3p	-7,97	0,024
hsa-miR-4677-3p	-7,66	0,044
hsa-miR-34a-3p	-7,23	0,030
hsa-let-7f-1-3p	-6,86	0,007
hsa-miR-6801-3p	**-6,62**	**0,017**
hsa-miR-503-5p	-6,52	0,006
hsa-miR-92a-1-5p	-6,32	0,000
hsa-miR-30d-3p	-6,24	0,047
hsa-miR-1307-5p	-5,74	0,021
hsa-miR-10a-5p	-5,59	0,031
hsa-miR-6511b-5p	-5,40	0,008
hsa-miR-503-3p	-5,23	0,034
hsa-miR-6862-5p	-5,04	0,017
hsa-miR-4689	-4,88	0,030
hsa-miR-3074-5p	-4,71	0,018
hsa-miR-1306-5p	-4,71	0,006
hsa-miR-3176	-4,37	0,020
hsa-miR-18a-5p	-4,37	0,020
hsa-miR-6511a-5p	-4,05	0,001
hsa-miR-139-5p	-3,80	0,024
hsa-miR-7-5p	-3,74	0,000
hsa-let-7d-5p	-3,68	0,004
hsa-miR-2355-3p	-3,61	0,010
hsa-miR-6749-3p	-3,42	0,021
hsa-miR-10a-3p	-3,39	0,002
hsa-miR-548ai hsa-miR-570-5p	-3,36	0,015
hsa-miR-6877-5p	-3,34	0,000
hsa-miR-7974	-3,34	0,008
hsa-miR-5587-3p	-3,30	0,049
hsa-miR-5094	-3,25	0,023
hsa-miR-1307-3p	-3,07	0,044
hsa-miR-1306-3p	-3,04	0,028
hsa-miR-30c-2-3p	-2,97	0,050
hsa-miR-33b-5p	-2,97	0,015
hsa-miR-19b-1-5p	**-2,89**	**0,038**
hsa-miR-147b	-2,87	0,007
hsa-miR-6800-3p	-2,81	0,050
hsa-miR-1278	-2,79	0,031
hsa-miR-365b-5p	-2,78	0,026
hsa-miR-2278	-2,71	0,013
hsa-miR-3174	-2,67	0,050
hsa-miR-449c-5p	-2,67	0,016
hsa-miR-3677-5p	-2,65	0,044
hsa-miR-3679-3p	-2,63	0,000
hsa-miR-651-5p	-2,58	0,000
hsa-miR-3677-3p	-2,58	0,003
hsa-miR-6797-3p	-2,52	0,006
hsa-miR-4723-5p	-2,49	0,011
hsa-miR-4685-3p	-2,48	0,008
hsa-miR-6762-3p	-2,43	0,030
hsa-miR-33b-3p	-2,39	0,001
hsa-miR-4523	-2,29	0,041
hsa-miR-6889-3p	-2,29	0,028
hsa-miR-378c	-2,24	0,037
hsa-miR-4485-5p	-2,19	0,002
hsa-miR-1286	-2,17	0,042
hsa-miR-6820-3p	-2,17	0,023
hsa-miR-4768-5p	**-2,16**	**0,005**
hsa-miR-378d	-2,12	0,022
hsa-miR-4640-3p	-2,11	0,014
hsa-miR-187-3p	-2,09	0,027
hsa-miR-4664-3p	-1,99	0,040
hsa-miR-3685	-1,98	0,031
hsa-miR-664b-5p	-1,93	0,043
hsa-miR-3187-3p	-1,91	0,018
hsa-miR-4786-5p	-1,89	0,046
hsa-miR-5587-5p	-1,87	0,003
hsa-miR-5697	-1,77	0,020
hsa-miR-378e	-1,74	0,028
hsa-miR-6858-3p	-1,74	0,048
hsa-miR-556-3p	-1,72	0,006
hsa-miR-320d	-1,70	0,049
hsa-miR-1915-5p	-1,68	0,006
hsa-miR-5091	-1,68	0,002
hsa-miR-4725-3p	-1,66	0,040
hsa-miR-4723-3p	-1,65	0,049
hsa-miR-3662	-1,64	0,006
hsa-miR-3188	-1,63	0,006
hsa-miR-6765-3p	-1,61	0,045
hsa-miR-3133	-1,61	0,028
hsa-miR-6842-3p	-1,55	0,043
hsa-miR-6850-3p	-1,51	0,014
hsa-miR-7112-5p	-1,49	0,028
hsa-miR-5680	-1,47	0,048
hsa-miR-1914-3p	-1,45	0,044
hsa-miR-6728-5p	-1,44	0,017
hsa-miR-5088-3p	-1,43	0,023
hsa-miR-6790-3p	-1,42	0,044
hsa-miR-129-5p	**-1,41**	**0,040**
hsa-miR-3664-3p	-1,41	0,000
hsa-miR-148a-3p	-1,40	0,009
hsa-miR-129-2-3p	-1,38	0,011
hsa-miR-1909-3p	-1,38	0,035
hsa-miR-135b-5p	-1,36	0,044
hsa-miR-320e	-1,36	0,013
hsa-miR-483-5p	-1,34	0,002
hsa-miR-1247-5p	-1,29	0,015
hsa-miR-3165	-1,25	0,012
hsa-miR-573	-1,24	0,015
hsa-miR-6850-5p	-1,24	0,044
hsa-miR-148a-5p	-1,20	0,002
hsa-miR-141-3p	-1,20	0,018
hsa-miR-548b-3p	-1,20	0,003
hsa-miR-5092	-1,19	0,026
hsa-miR-6880-5p	-1,18	0,017
hsa-miR-335-3p	-1,18	0,002
hsa-miR-4697-3p	-1,17	0,020
hsa-miR-135b-3p	-1,16	0,045
hsa-miR-676-3p	-1,15	0,006
hsa-miR-1273d	-1,15	0,048
hsa-miR-3131	-1,15	0,019
hsa-miR-200b-3p	**-1,14**	**0,047**
hsa-miR-200a-5p	-1,14	0,014
hsa-miR-200a-3p	-1,14	0,005
hsa-miR-200b-5p	-1,13	0,042
hsa-miR-429	**-1,12**	**0,046**
hsa-miR-3116	-1,06	0,012
hsa-miR-6891-5p	-1,06	0,030
hsa-miR-3121-3p	-1,02	0,027
hsa-miR-376a-3p	-1,02	0,045
hsa-miR-499a-3p	-1,01	0,013
hsa-miR-543	-1,01	0,047
hsa-miR-1229-5p	-0,99	0,041
hsa-miR-377-5p	-0,97	0,019
hsa-miR-134-5p	-0,94	0,027
hsa-miR-1913	-0,90	0,027
hsa-miR-495-3p	**-0,88**	**0,000**
hsa-miR-485-3p	-0,82	0,017
hsa-miR-1250-5p	-0,81	0,039
hsa-miR-382-3p	-0,80	0,026
hsa-miR-3936	-0,80	0,023
hsa-miR-154-5p	-0,80	0,036
hsa-miR-4440	-0,79	0,041
hsa-miR-129-1-3p	-0,78	0,005
hsa-miR-4783-3p	-0,78	0,010
hsa-miR-376b-3p	-0,78	0,030
hsa-miR-4802-3p	-0,77	0,007
hsa-miR-329-3p	-0,76	0,001
hsa-miR-203a-3p	-0,72	0,034
hsa-miR-203a-5p	-0,71	0,001
hsa-miR-205-3p	-0,69	0,017
hsa-miR-3935	-0,61	0,012

Supplementary Table 2B. List of down-regulated miRNAs. miRNA expression profile significantly differs in PC3 exposed for 3 days to CM-CAFs compared to CM-HPFs. Fold change (FC) variations $\geqslant$1.5 and $\leqslant$−1.5 of the differentially expressed (DE) miRNAs were used to define up- and down-regulated miRNAs, respectively. Out of the 1276 deregulated miRNAs, 302 showed a p-value <0.05; 149 miRNAs showed log2 Ratio $\leqslant$ -0.6 (fold change $\leqslant$-1.5). Grey boxes indicate miRNAs predicted to target DNMT3A.

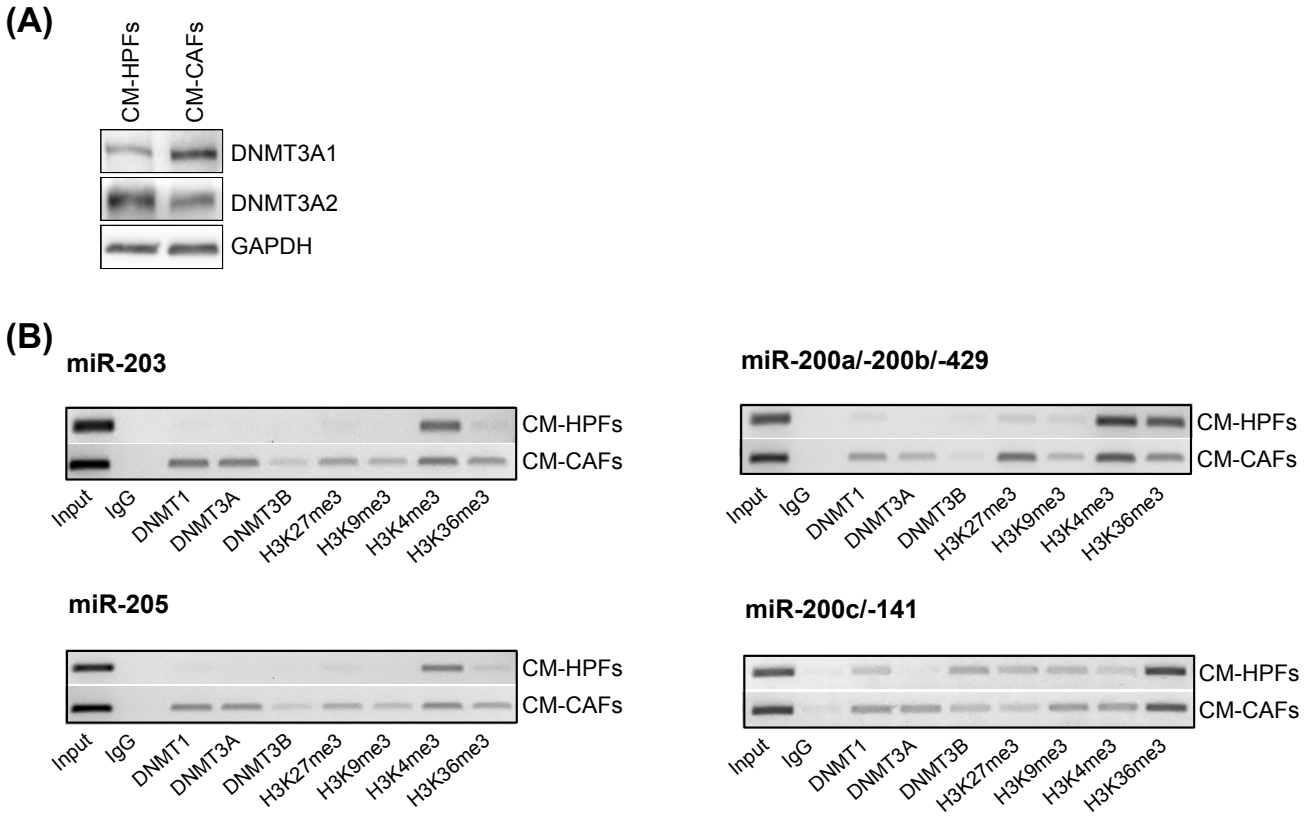

Supplementary Figure 1. (A) Western Blot analysis of DNMT3A isoforms. Specific antibodies recognizing isoform a and b were used to evaluate the shift between the isoforms of DNMT3A. Densitometric analysis on the bands has been performed for each experiment (for a total of three experiments), and used to determine averages/standard deviations shown in Figure 1A. Pictures are representative of the average alterations of all independent experiments (**B) PCR products following ChIP experiments.** The pictures represent the products of the amplifications of the immunoprecipitated DNA, and are representative of the average alterations. Each experiment was reproduced in triplicate. Densitometric analysis on the bands has been performed for each experiment, and used to determine averages/standard deviations shown in Figure 2.

(A)

miRNA	Log Ratio CAF/HPF	t test CAF/HPF
hsa-miR-29b-3p	-0,607	0,288
hsa-miR-29a-3p	-0,171	0,330
hsa-miR-29c-3p	0,095	0,679

(B)

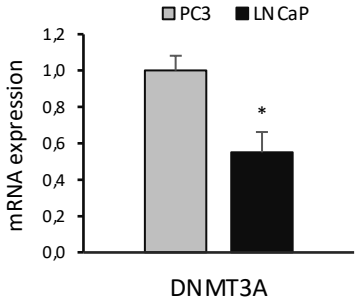

(C)

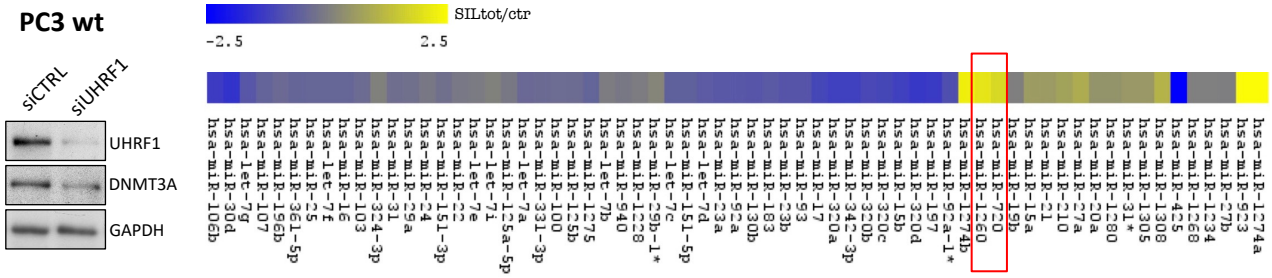

Supplementary Figure 2. (A) Alteration of the miR-29 family by RNA -seq. All three most represented members of the -29 family were detected in our RNA-sequencing analysis, but their alteration were not statistically significant. (**B) Expression levels of DNMT3A in PC3 wild-type and LNCaP cell lines**. The histograms show the levels of DNMT3A (pan) mRNA. (**C) Profile of altered miRNAs following UHRF1-dependent regulation of DNMT3A.** Silencing of UHRF1 in PC3 cells resulted in reduction of DNMT3A levels. miRNA profile analysed through human microarray (Microarray System labelling kit V2, Agilent) showed various altered miRNAs; among them, miR-1260a and miR-720 are the only predicted to target DNMT3A. miR-720 was not significantly altered in our *ex-vivo* EMT model.

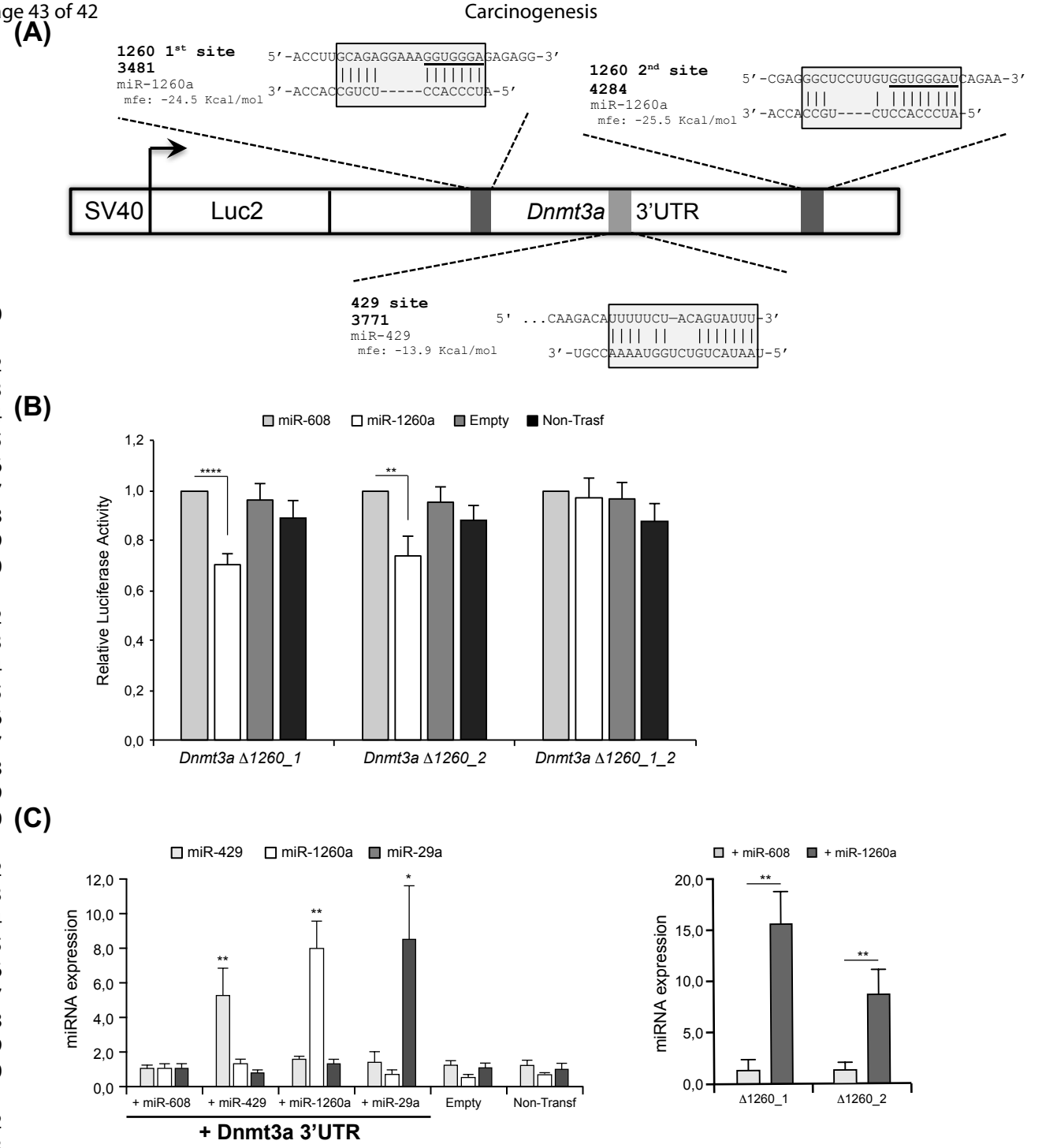

Supplementary Figure 3. (A) Schematic location of miRNA target sites in Dnmt3a 3'UTR. Schematic representation of pGL4.13 reporter plasmid harboring wild-type and mutated forms of Dnmt3a 3'UTR used to generate luciferase constructs. Sequences of the predicted sites recognized by miR-1260a and miR-429 are shown and deletions are underlined. Base-pairing and stability of miRNA/mRNA pairings, calculated as minimum free energy (mfe) with the RNAhybrid tool, are also indicated**. (B) Functional analysis of miR-1260a binding to *Dnmt3a*-3'UTR.** PC3 cells were co-transfected with *Dnmt3a*-3'UTR luciferase constructs harbouring deletions in the complementary sequence to miR-1260a target sites (Δ1260_1 and Δ1260_2), and with psiUx-miR-1260a or psiUx-miR-608. Luciferase activity was assessed 24h after transfection (N=4; Student's t test: **p<0.01, ***p<0.001). Empty = psiUx-empty; Non-transf = non transfected cells **(C) Expression levels of miR-1260a and miR-429 following co-transfection.** miRNA levels were assessed in PC3 cells following co-transfection with *Dnmt3a*-3'UTR WT luciferase constructs and with psiUx-miR-1260a or psiUx-miR-429 overexpressing plasmids. psiUx-miR-608 and psiUx-miR-29a were used as negative and positive controls, respectively. miRNA levels were also assessed in PC3 cells following co-transfection of the over-expressing psiUx-miR-1260a or psiUx-miR-608 plasmids and the two *Dnmt3a*-3'UTR mutants (Δ1260_1 and Δ1260_2). Empty = psiUx-empty; Non-transf = non transfected cells

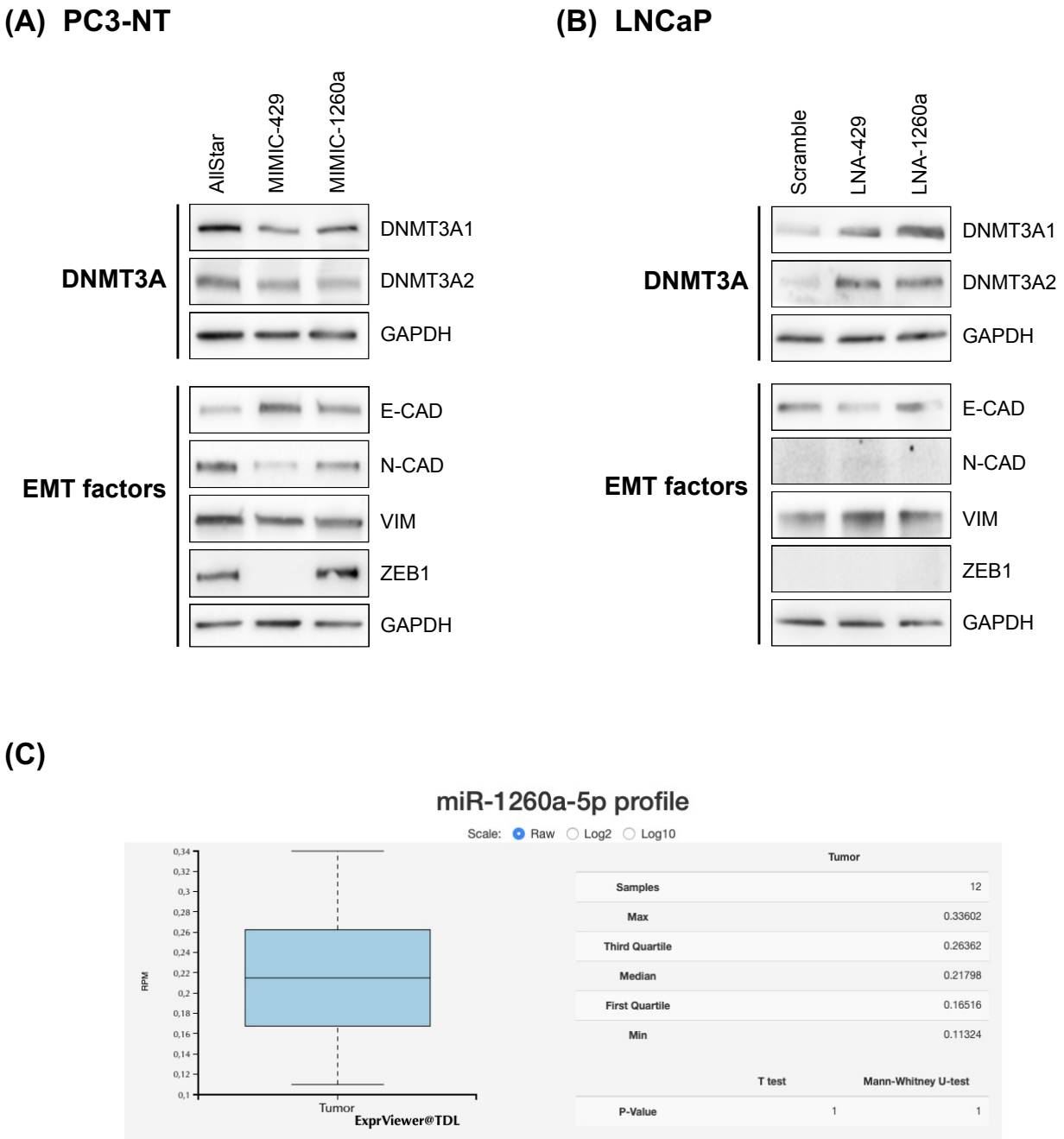

Supplementary Figure 4. (A-B) Western Blot analysis of DNMT3A isoforms and EMT factors. (A) Over-expression of miR-429 or miR-1260a in PC3 cells. (B) Inhibition of miR-429 or miR-1260a in LNCaP cells. Western Blot pictures, representative of the average alterations of four independent experiments, show the levels of DNMT3A (isoform a, DNMT3A1, and isoform b, DNMT3A2) and of key EMT factors following overexpression or inhibition of miR-429 and miR-1260a in PC3 and LNCaP, respectively. **(C) miR-1260a expression in the complete TCGA-PRAD dataset.** miR-TV (a web interface to query the miRNA information of the TCGA dataset; http://mirtv.ibms.sinica.edu.tw/analysis.php) interrogation shows that miR-1260a was detected in 12 PCa patients. Among the 87 presenting an EMT-like or MET-like signature, miR-1260a was expressed in 1 patient only. miR-1260a has not been detected in normal prostate samples.